AGU
ADVANCING EARTH AND SPACE SCIENCE

Tectonics®

Insights of Active Extension Within a Collisional Orogen From GNSS (Central Betic Cordillera, S Spain)

I. Martin-Rojas[1] [iD], P. Alfaro[1], J. Galindo-Zaldivar[2,3] [iD], M. J. Borque-Arancón[4,5], F. J. García-Tortosa[5,6], C. Sanz de Galdeano[3], M. Avilés[5], A. Sánchez-Alzola[7] [iD], L. González-Castillo[2], P. Ruano[2,3] [iD], I. Medina-Cascales[1] [iD], V. Tendero-Salmerón[2] [iD], A. Madarieta-Txurruka[2] [iD], M. T. Pedrosa-González[2], and A. J. Gil-Cruz[4,5]

[1]Dpto. De Ciencias de la Tierra y del Medio Ambiente, Universidad de Alicante, Alicante, Spain, [2]Departamento de Geodinámica, Facultad de Ciencias, Universidad de Granada, Granada, Spain, [3]Instituto Andaluz de Ciencias de la Tierra (CSIC-Universidad de Granada), Granada, Spain, [4]Departamento Ing. Cartográfica, Geodésica y Fotogrametría, Universidad de Jaén, Jaén, Spain, [5]Centro de Estudios Avanzados en Ciencias de la Tierra, Energía y Medio Ambiente (CEACTEMA), Universidad de Jaén, Jaén, Spain, [6]Departamento de Geología, Facultad de Ciencias, Universidad de Jaén, Jaén, Spain, [7]Departamento de Estadística e Investigación Operativa, Universidad de Cádiz, Puerto Real, Spain

Abstract The coexistence of shortening and extensional tectonic regimes is a common feature in orogenic belts. The westernmost end of the Western Mediterranean is an area undergoing shortening related to the 5 mm/yr NNW–SSE convergence of the Nubia and Eurasia Plates. In this region, the Central Betic Cordillera shows a regional ENE–WSW extension. Here, we present GNSS-derived geodetic data along a 170 km-long transect orthogonal to the main active normal faults of the Central Betic Cordillera. Our data indicate that the total extension rate along the Central Betic Cordillera is 2.0 ± 0.3 mm/yr. Extension is accommodated in the eastern (0.8 ± 0.3 mm/yr in the Guadix-Baza Basin) and western (1.3 ± 0.3 mm/yr in the Granada Basin) parts of the Central Betic Cordillera, while no extension is recorded in the central part of the study area. Moreover, our data permit us to quantify, for the first time, short-term fault slip rates of the Granada Fault System, which is one of the main seismogenic sources of the Iberian Peninsula. We deduce a fault slip rate of $\sim 1.3 \pm 0.3$ mm/yr for the whole Granada Basin, with 0.9 ± 0.3 mm/yr being accommodated in the Granada Fault System and 0.4 ± 0.3 mm/yr being accommodated in the southwestern sector of the Granada Basin, where no active faults have been previously described at the surface. The heterogeneous extension in the Central Betic Cordillera could be accommodated by shallow high-angle normal faults that merge with a detachment at depth. Part of the active extension could be derived from gravitational instability because of underlying over-thickened crust.

Plain Language Summary We present here high-precision GPS data obtained in S Spain. In this area tectonic deformation of the Earth crust is related to the convergence between Nubia (Africa) and Eurasia Plates. Under this general convergence setting, our study area is undergoing extensional deformation. GPS data permit us to quantify and characterize this extension. The total extension in our study area is 2.0 ± 0.3 mm/yr. But this extension is heterogeneous, as it concentrates in two areas to the east and to the west, separated by a zone with no extension. Moreover, our data permit to quantify, for the first time, short-term fault slip rates of the Granada Fault System (0.9 ± 0.3 mm/yr). This parameter is essential to characterize the seismic hazard of this structure, which is one of the main seismogenic sources of the Iberian Peninsula. We also discuss the subsurface geometry of the faults accommodating this heterogeneous extension and the crustal mechanism responsible for that.

1. Introduction

The peri-Mediterranean orogenic belt started to form as a consequence of widespread subduction processes related to the onset of the Nubia-Eurasia convergence. From the Eocene on, these subduction-dominated dynamics changed, leading to a tectonic setting in which the formation of mountain belts near the subduction trenches was coeval with the opening of back-arc basins and the formation of orogenic arcs. This change was the consequence of fast slab retreat throughout the Mediterranean region (see compilation in Jolivet and Faccenna (2000) and Jolivet et al. (2021)).

This mixed tectonic setting is still active in the Eastern Mediterranean region, where widespread extension is presently occurring in the Corinth or Western Anatolian rifts (Aktug et al., 2009; Armijo et al., 1999; Ford

Investigation: I. Martin-Rojas, P. Alfaro, J. Galindo-Zaldivar, M. J. Borque-Arancón, F. J. García-Tortosa, C. Sanz de Galdeano, M. Avilés, A. Sánchez-Alzola, L. González-Castillo, P. Ruano, I. Medina-Cascales, V. Tendero-Salmerón, A. Madarieta-Txurruka, M. T. Pedrosa-González, A. J. Gil-Cruz
Methodology: I. Martin-Rojas, P. Alfaro, J. Galindo-Zaldivar, M. Avilés, A. Sánchez-Alzola, A. J. Gil-Cruz
Project Administration: I. Martin-Rojas, A. J. Gil-Cruz
Resources: I. Martin-Rojas, P. Alfaro, J. Galindo-Zaldivar, A. J. Gil-Cruz
Supervision: I. Martin-Rojas, A. J. Gil-Cruz
Validation: I. Martin-Rojas, P. Alfaro, J. Galindo-Zaldivar, A. J. Gil-Cruz
Visualization: I. Martin-Rojas
Writing – original draft: I. Martin-Rojas, I. Medina-Cascales, A. J. Gil-Cruz
Writing – review & editing: I. Martin-Rojas, P. Alfaro, J. Galindo-Zaldivar, A. Madarieta-Txurruka, A. J. Gil-Cruz

et al., 2007, 2017; Gawthorpe et al., 2018; Rohais et al., 2007; Taylor et al., 2011). In the Betic Cordillera (Figure 1), located in the Western Mediterranean region, extensive extension started to end 8 Ma ago (Billi et al., 2011; Crespo-Blanc et al., 1994; d'Acremont et al., 2020; Faccenna et al., 2014; Galindo-Zaldivar & Jabaloy, 1989; Jabaloy et al., 1992, 1993; Medaouri et al., 2014). Therefore, this region is generally understood as an area undergoing shortening related to convergence between the Nubian and Eurasian plates. Within this general convergence geodynamic cadre, three major tectonic sectors are recognized in the Betic Cordillera (Figure 1): (a) the Eastern Betic Cordillera, dominated by transpressive tectonics, (b) the Western Betic Cordillera, dominated by shortening, and (c) the Central Betic Cordillera, an area undergoing extension.

In the Eastern Betic Cordillera, the Eurasia-Nubia convergence is effectively transferred because of a tectonic indenter (Figure 1) (Borque et al., 2019; Coppier et al., 1989; Estrada et al., 2018; Galindo-Zaldivar et al., 2022; Palano et al., 2015; Tendero-Salmerón, 2022). This convergence is accommodated along a transpressive tectonic corridor: the Trans-Alboran Shear Zone (Bousquet, 1979; De Larouziere et al., 1987), also named the Eastern Betic Shear Zone (Silva et al., 2003). Several regional geodetic studies have quantified both the regional and local slip rates of this left-lateral shear zone (Borque et al., 2019; Echeverria et al., 2013, 2015).

In the Western Betic Cordillera, NW–SE shortening is the result of westwards displacement of the cordillera with respect to the relatively stable foreland (Gonzalez-Castillo et al., 2015). This shortening, accommodated by active folding and faulting, has been quantified by regional geodetic studies (Gonzalez-Castillo et al., 2015; Serpelloni et al., 2007).

Nevertheless, in this convergence setting of the Eurasian-Nubia plates, the Central Sector of the Betic Cordillera is characterized by active NE–SW extension (Figure 1). Studies on active tectonics describe NW–SE active normal faults in the Granada and Guadix-Baza Basins (Alfaro et al., 2001, 2008, 2021; Castro et al., 2018; Galindo-Zaldívar et al., 1999; Gil et al., 2002; Medina-Cascales et al., 2020, 2021; Rodriguez-Fernandez & Sanz de Galdeano, 2006; Ruiz et al., 2003; Sanz de Galdeano & López-Garrido, 1999; Sanz de Galdeano et al., 2012, 2020; and many others) (Figure 2). This extension is further confirmed by seismic studies, as seismic moment tensors are compatible with NE–SW regional extension (Galindo-Zaldívar et al., 1999; Herráiz et al., 2000; Palano et al., 2015; Stich et al., 2006, 2007) (Figure 1). Moreover, a significant amount of seismic activity in the Granada Basin is attributed to NW–SE normal faults (Madarieta-Txurruka et al., 2021; Morales et al., 1997; Reicherter et al., 2003; Ruano et al., 2004; Sanz de Galdeano et al., 2003).

The extension rates of the Central Betic Cordillera have been estimated from broad regional geodetic studies (Galindo-Zaldivar et al., 2015; Palano et al., 2015; Pérez-Peña et al., 2010; Serpelloni et al., 2007; Stich et al., 2006). Stich et al. (2006) estimated an extension rate of ~2.5 mm/year in a N60°E direction. Serpelloni et al. (2007) indicated that the Alboran-Betics region accommodates ~2.1 ± 0.7 mm/year of E–W extension. Pérez-Peña et al. (2010) showed an extension of ~3.7 mm/year in a WSW–ENE direction for the whole Betic Cordillera. Other geodetic studies quantified the local extension rates of some of the main active faults within the Central Betic Cordillera (Alfaro et al., 2021; Gil et al., 2002, 2017). This active deformation is responsible for significant seismicity, such as the 1884 Andalusia earthquake (I = VIII-IX, M_{ms} = 6.5) (Reicherter et al., 2003), the 1531 Baza earthquake (I = VIII–IX; Mw = 6.0) (Alfaro et al., 2008), and the 2021 Granada seismic swarm (Madarieta-Txurruka et al., 2021, 2022).

In this work, we present GNSS-derived geodetic deformation data along a 170-km-long transect orthogonal to the main active normal faults of the Central Betic Cordillera. Our results permit us to quantify regional extensional rates and to analyze deformation partitioning within this region. Moreover, our study assigns short-term slip rates to some of the main active faults in this area. The comparison of our short-term slip rates with geologically derived long-term rates sheds further light on how deformation is distributed. We also discuss further implications for fault geometries and possible crustal mechanisms for explaining this extension. Finally, our results will be the basis of future seismic hazard assessments for this region, with significant seismicity.

1.1. Geodynamic and Geological Setting

The Betic Cordillera is located at the Nubia-Eurasia plate boundary (Figure 1). This sector is under N–S to NW–SE convergence, probably since the Late Cretaceous (Dewey et al., 1989; Mazzoli & Helman, 1994; Rosenbaum et al., 2002; Srivastava et al., 1990). At present, the Nubian and Eurasian plates converge at a rate of approximately 5–6 mm/year according to regional models (DeMets et al., 1994; McClusky et al., 2003; Nocquet, 2012; Nocquet & Calais, 2003; Pérez-Peña et al., 2010; Serpelloni et al., 2007; Stich et al., 2006).
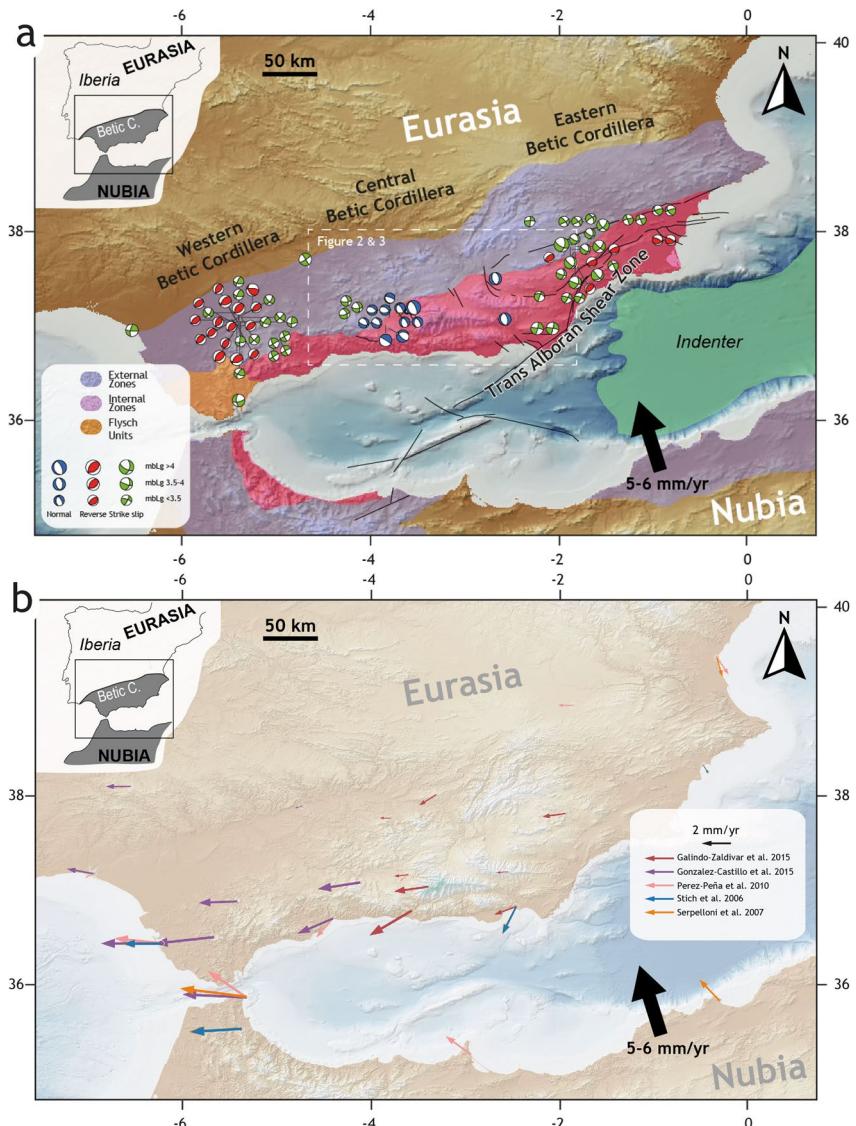
Figure 1. (a) Simplified geological map of SE Iberia and N Africa, showing the three major sectors recognized in the Betic Cordillera. Focal mechanisms (Instituto Geográfico Nacional, 2022) show how the Western Betic Cordillera undergoes shortening, the Eastern Betic Cordillera strike-slip and the Central Betic Cordillera is dominated by extension. (b) Regional velocity field derived from cGNSS data (after Serpelloni et al. (2007), Pérez-Peña et al. (2010), Galindo-Zaldivar et al. (2015), and González-Castillo et al. (2015)) respect to the Eurasia fixed reference frame (IGb_08).

Under this general plate convergence, the Betic Cordillera underwent a complex geodynamic evolution. After an initial period characterized by subduction-related shortening, during the Early to Middle Miocene, the Betic Internal Zones underwent general NE–SW to E–W extension. This extension was the consequence of fast slab retreat and subsequent development of a back-arc basin (Galindo-Zaldivar et al., 2015; Gonzalez-Castillo et al., 2015; Gutscher et al., 2002; Mancilla et al., 2015). Miocene extension was accommodated by ductile deformation evolving into brittle low-angle normal faults, such as the Mecina Fault, which separates the two lowermost metamorphic complexes of the Betic Cordillera and shows top-to-the-W kinematics (Galindo-Zaldivar & Jabaloy, 1989). During the Upper Miocene, the general geodynamic setting changed. From that moment onwards, the Betic Cordillera has been dominated by the convergence between the Nubia and Eurasia Plates. This convergence produces NNW–SSE shortening, which is responsible for the main topographic features observed today (Sanz de Galdeano & Alfaro, 2004). After that geodynamic change, only the Central Betic Cordillera underwent extension, accommodated by NNW–SSE to WNW–ESE high-angle normal faults (Alfaro et al., 2008; Azañón et al., 2004; Castro et al., 2018; García-Tortosa et al., 2008; Medina-Cascales et al., 2020; Sanz de Galdeano et al., 2012). These normal faults produced half-grabens
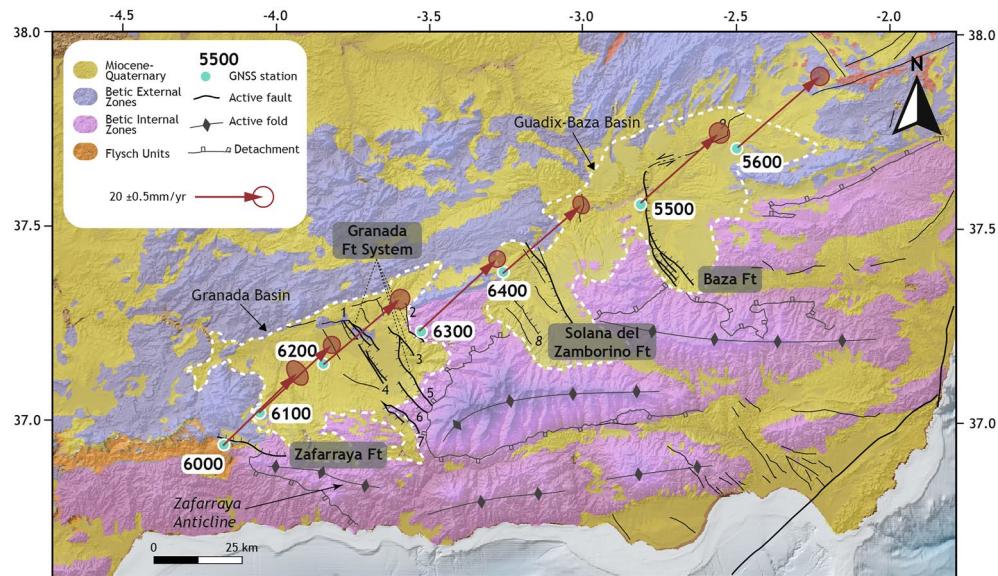
**Figure 2.** Simplified geological map of the Central Betic Cordillera. Black lines indicate the main (thick) and minor (thin) active normal faults. Green dots are our GNSS stations. Arrows indicate the absolute velocity field of the Central Betic Cordillera derived from the position time series and 95% confidence ellipses. 1, Sierra Elvira Fault; 2, Alfacar Fault; 3, Fargue Fault; 4, Santa Fe Fault; 5, Granada Fault; 6, Dilar Fault; 7, Padul Fault; 8, Graena Fault; 9 Galera Fault.

in their hanging walls filled by Upper Miocene to Quaternary sediments and, hence, led to the development of Neogene-Quaternary sedimentary basins, including the Granada and Guadix-Baza Basins (Figure 2). These normal faults comprise the Granada Fault System (including the Sierra Elvira, Santa Fe, Dilar, Granada, Fargue, Alfacar, and Padul Faults) (Alfaro et al., 2001; Azañón et al., 2004; Calvache et al., 1997; Estevez & Sanz de Galdeano, 1983; Lhénaff, 1965; Morales et al., 1990; Riley & Moore, 1993; Rodriguez-Fernandez & Sanz de Galdeano, 2006; Ruano et al., 2004; Sanz de Galdeano & López-Garrido, 1999) that generated the Granada Basin.

The Baza Fault (Figure 2) is another of these high-angle normal faults (Alfaro et al., 2008; Castro et al., 2018; Fernández-Ibáñez et al., 2010; García-Tortosa et al., 2008; Medina-Cascales et al., 2020; Sanz de Galdeano et al., 2012); this active structure is responsible for the development of the eastern sector of the Guadix-Baza Basin. Other normal faults in the Central Betic Cordillera are the Solana del Zamborino Fault and the Graena Fault (Sanz de Galdeano et al., 2012) (Figure 2). The WNW–ESE-striking Zafarraya Fault is located at the SW end of our study area (Galindo-Zaldivar et al., 2003; Gil et al., 2002; Reicherter et al., 2003) (Figure 2).

Active normal faults in the Central Betic Cordillera are the seismogenic sources of significant and destructive earthquakes. The Zafarraya Fault is probably responsible for the well-known 1884 Andalusia Earthquake (I = VIII–IX, M_{ms} = 6.5) (Galindo-Zaldivar et al., 2003; Reicherter et al., 2003). The Granada Fault System is responsible for the 1431 Otura-Alhendín earthquake as well as the 1806 Pinos SW of Armilla and 1956 Albolote Earthquakes. This fault system also produced the 2021 Granada Seismic Swarm (Lozano et al., 2022; Madarieta-Txurruka et al., 2021, 2022). The Baza Fault is the seismogenic source of the 1531 Baza earthquake (I = VIII–IX, M_{ms} = 6.0) (Alfaro et al., 2008).

Several geodynamic models have been proposed to explain the present geodynamic setting of the Betic Cordillera, which is characterized by coeval extension and shortening. While shortening is widely attributed to convergence between the Nubian and Eurasian plates, the origin of the extension is under debate. Two main hypotheses are evoked to explain the extension in the Central Betic Cordillera: (a) eastwards Nubia plate subduction and subsequent back-arc extension associated with westwards slab roll-back (Galindo-Zaldivar et al., 2015; Gonzalez-Castillo et al., 2015; Lonergan & White, 1997; Royden, 1993), and (b) lithospheric delamination of a previous overthickened crust (Mancilla et al., 2013; among others).

1.2. GNSS Sites and Data Processing

Several local episodic GNSS networks already exist in the Central Betic Cordillera: the Granada Basin Network (Gil et al., 2002), Padul Fault Network (Ruiz et al., 2003), Zafarraya Fault—Sierra Tejeda Antiform Network

Table 1
East and North Absolute and Residual Velocities Estimated at the Profile Sites

Site ID	Velocity (mm yr⁻¹)		Uncertainty (mm yr⁻¹)		Res. velocity (mm yr⁻¹)	
	East	North	East	North	East	North
6000	17.1	16.7	±0.3	±0.5	−2.8	0.1
6100	16.9	15.8	±0.2	±0.2	−3.0	−0.8
6200	17.8	15.2	±0.3	±0.2	−2.2	−1.3
6300	18.1	16.5	±0.2	±0.3	−1.9	−0.1
6400	18.3	16.0	±0.2	±0.3	−1.7	−0.6
5500	18.2	16.3	±0.3	±0.3	−1.8	−0.3
5600	19.0	16.4	±0.2	±0.2	−1.0	−0.1

(Galindo-Zaldivar et al., 2003), and Baza Fault Network (Alfaro et al., 2021). We used some stations of these networks to establish and measure a new regional profile along a transect involving most of the Central Betic Cordillera (Figure 2). This ENE–WSW GNSS transect involves two stations from the Zafarraya Fault and Sierra Tejeda Antiform Networks, two from the Granada Basin Network and two from the Baza Fault Network. Additionally, a new station has been added, resulting in a total of seven geodetic stations involved in the study geodetic transect.

Sites 6000 and 6100 belong to the Zafarraya Fault and Sierra Tejeda Antiform Networks. They are located on the basement of the Central Betic Cordillera (Betic External Zones) (Figure 2). Station 6200 belongs to the Granada Basin network and is located on the Neogene sediments of the basin infill. Station 6300 is located just inside the NE border of the Granada Basin on rocks belonging to the Central Betic Cordillera basement (Betic Internal Zones). Station 6400 is situated on basement rocks (Betic External Zones) at the western limit of the Guadix-Baza Basin. Site 5500 is on basement rocks (Betic Internal Zones) outcropping in the center of the Guadix-Baza Basin. Finally, station 5600 is at the southeastern limit of the Guadix-Baza Basin on basement rocks (Betic External Zones).

Every GNSS site consists of a benchmark or a pillar anchored to solid rock. To measure with a benchmark, a 50 cm long aluminum tube is screwed on it, and the GNSS antenna is set up on top. Alternatively, three stations are geodetic pillars with a force centring device. Sites 6100, 6400, 5500, and 5600 are benchmarks, and sites 6000, 6200, and 6300 are geodetic pillars. Episodic surveys of the geodetic profile were carried out in 2009, 2010, 2011, 2012, and 2017. Some sites were also observed in 2015 and 2016. During each survey, the sites were continuously observed for four-day intervals (96 hr). During the 2009 and 2010 campaigns, the GPS receivers used were Leica Geosystem GX1230 receivers and LEIAX1202 antennas, whereas in subsequent campaigns in 2011, 2012, 2015, 2016, and 2017, the equipment was Leica Geosystem AR10 receivers and LEIAR10 antennas.

The data processing was performed by Precise Point Positioning using GipsyX software (Bertiger et al., 2020a, 2020b). GipsyX is GNSS-inferred positioning software developed by the Jet Propulsion Laboratory (JPL) and maintained by the Near-Earth Tracking Applications and Systems groups. A similar standard procedure for all campaigns was used. All the JPL products were computed in the same IGb14 reference frame.

1.3. Velocity Field

After processing all daily data with GipsyX in the IGb14 reference frame the time series were displayed (Figure S1). For our calculations, we considered the change in GPS antennas and receivers between the 2010 and 2011 campaigns, which produced a slip in the time series. The estimation of the crustal velocity field is computed from the IGb14 time series by using the Time Series Analysis Software SARI (Santamaría-Gómez, 2019). In our case, the model applied consists of an intercept, a site rate and an offset to account for antenna change. The uncertainties are computed using a colored noise model. The error term is composed of white noise and temporally correlated random error. The colored noise is described by a random walk process. We assumed a typical magnitude for this process of 1.0 mm/$\sqrt{\text{yr}}$. Table 1 shows the absolute velocities and residual velocities calculated with respect to a fixed Eurasia as defined by the ITRF2014 plate motion model (Altamimi et al., 2017). Figure 2 shows the present-day GNSS-derived absolute velocity vectors and 95% confidence error ellipses, and Figure 3a shows
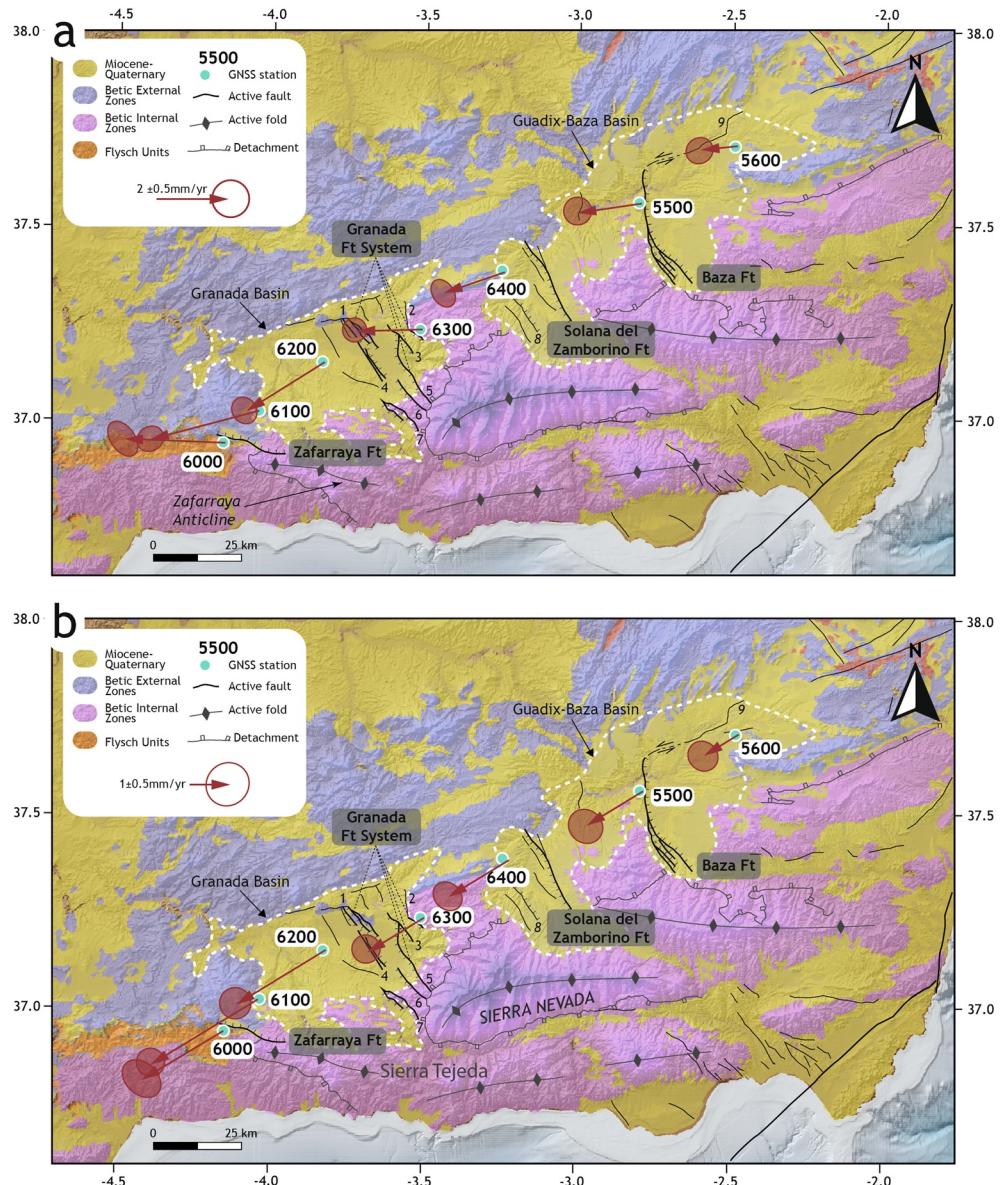
Figure 3. GNSS residual velocities of the Central Betic Cordillera. (a) With respect to a fixed Eurasia as defined by the ITRF2014 plate motion model (Altamimi et al., 2017) and 95% confidence ellipses. (b) Projected along the N060E direction and 95% confidence ellipses. The SW increase in the vectors module indicate a regional SW-NE extension.

the residual velocity field with respect to a fixed Eurasia. Furthermore, we projected the residual velocity vectors along the N060E direction (Figure 3b). This direction is subperpendicular to the mean strike of the major active faults in the study area (Figure 3b).

2. Discussion

2.1. Tectonic Deformation Rates in the Betic Cordillera

The Betic Cordillera undergoes active extension and shortening that should be quantified to better understand the present-day behavior of the Nubia-Eurasia plate boundary. In the Western Betic Cordillera, previous cGNSS regional data indicate a total E–W shortening up to 2.6 ± 0.1 mm/yr (Gonzalez-Castillo et al., 2015). In the Eastern Betic Cordillera, transpressive NNW–SSE rates range between 0.7 and 1.5 ± 0.1 mm/yr (Borque et al., 2019; Echeverria et al., 2013, 2015). In the case of the Central Betic Cordillera, our GNSS-derived velocity field sheds light on the overall regional deformation that is currently occurring in this tectonic domain. A general
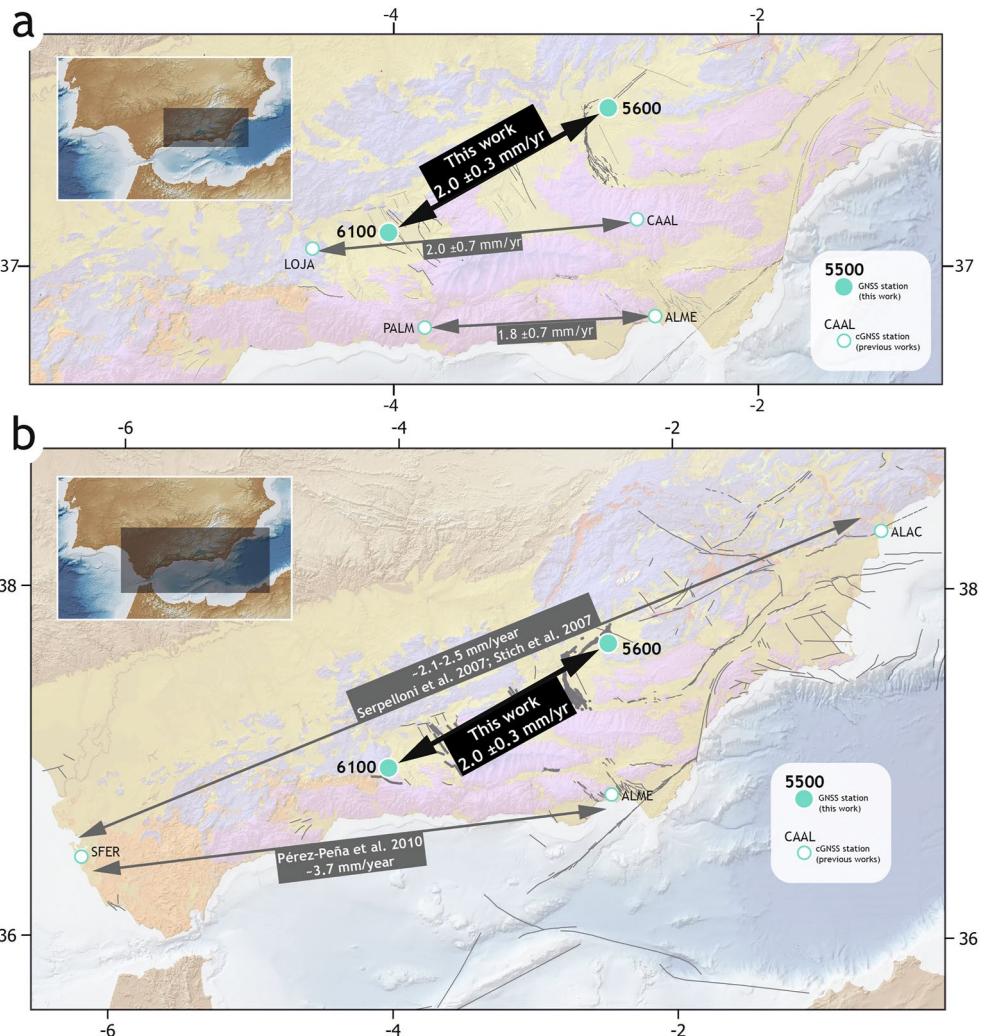
Figure 4. Comparison between the extension rate derived from our episodic GNSS network and regional extension rates derived from cGNSS data after Galindo-Zaldivar et al. (2015) (a) and Serpelloni et al. (2007) and Pérez-Peña et al. (2010) (b).

increase to the SW of the absolute value of the N060E components of the velocity vectors is observed between stations 5600 and 6100 (Table 1, Figure 3b). This indicates that this transect is undergoing extension. Subtraction of the N060E components of stations 5600–6100 shows that the extension in this area is 2.0 ± 0.3 mm/yr (Table 1, Figure 3b). This value is in good agreement with previously reported extension rates for the Central Betic Cordillera. Galindo-Zaldivar et al. (2015) presented cGNSS-derived velocity vectors for several stations within the Central Betic Cordillera (Figure 4a). We quantified the overall extension from these cGNSS data following the same procedure described above for our own vectors. The distribution of the stations presented by Galindo-Zaldivar et al. (2015) permits the analysis of the overall extension of the Central Betic Cordillera along two transects: one involving stations CAAL-LOJA and the other involving stations ALME-PALM. The subtraction of the N060E component of the velocity vectors for stations along these two transects yields extension rates of 2.0 ± 0.7and 1.8 ± 0.7 mm/yr, respectively. These values are very similar to the value of 2.0 ± 0.3 mm/yr that we obtained from our episodic study. Therefore, we consider this value (2.0 ± 0.3 mm/yr) to be representative of the total extension that is presently occurring in the Central Betic Cordillera. This extension rate also agrees with regional extension rates proposed by broad studies carried out on the Nubia-Eurasia plate boundary, ranging between 2.1 and 3.7 mm/yr (Pérez-Peña et al., 2010; Serpelloni et al., 2007; Stich et al., 2006) (Figure 4b). Some authors proposed higher deformation rates for this area (Pérez-Peña et al., 2009) based on the offset of a geomorphological marker. However, this marker was later reinterpreted as older (García-Tortosa et al., 2011), and therefore, deformation rates should also be reduced within the abovementioned range. The extensional deformation

affects up to 6100, although a comparison between the 6100 and 6000 stations, in the southwesternmost part of the profile, shows the change in behavior to shortening (Figure 3).

2.2. Fault Slip Rates in the Central Betic Cordillera

Our GNSS results permit us to better constrain the fault slip rates of the main active structures in this region. For this analysis, we assumed a rigid-block approach (Alfaro et al., 2021; Borque et al., 2019), where all the observed deformation is accommodated by the active faults. This approach considers that all horizontal deformation is accommodated by the active faults located between the analyzed stations. That is, we assume that no internal deformation takes place within the blocks bounded by active faults. Under this assumption, we derived fault slip rates by transforming the horizontal deformation field into along-fault displacement (slip rate), using the fault kinematics (pure normal kinematics for all the faults in our study area) and fault dip.

2.3. Fault Slip Rates in the Guadix-Baza Basin

If we subtract the N060E component of stations 5600-5500, we obtain a horizontal extension rate of 0.7 ± 0.4 mm/yr (Table 1 and Figure 3b). The only active fault between these two stations is the Baza Fault (Figures 2 and 3b). Assuming pure normal kinematics and a fault dip ranging between 45° and 60°, we transformed the 0.7 ± 0.4 mm/yr of horizontal extension rate into a fault-slip rate. After this calculation we derived a short term slip rate for the Baza Fault ranging between 0.9 ± 0.3 and 1.3 ± 0.4 mm/yr (assuming dips of 45° and 60°, respectively). These values are in agreement with previously reported slip rates, ranging between 0.3 ± 0.3 and 1.3 ± 0.4 mm/yr using data from a local episodic GNSS network (Alfaro et al., 2021).

The comparison of the N060E component of stations 5500–6400 yields a horizontal extension rate of 0.1 ± 0.4 mm/yr (Table 1 and Figure 3b). In that case, we assumed that this extension is accommodated by the Solana del Zamborino Fault (Figure 2). No previous short-term slip rate has been reported for this fault. We are aware that the computed value is not statistically significant because of the very low signal-to-noise ratio. However, if we assume this value to be a very rough approximation of the horizontal extension rate accommodated by the Solana del Zamborino Fault, we can compute the fault slip rate following the same procedure previously discussed. We obtained a fault slip rate of this active structure that could be approximately 0.1 mm/yr. These results are in good agreement with geological and geomorphological data, as the Solana del Zamborino Fault presents a subtle geomorphic expression (Sanz de Galdeano et al., 2012). Moreover, our data are also in agreement with previously reported long-term slip rates, ranging between 0.1 and 0.3 mm/yr (assuming a dips of 45° and 60°, respectively) (Sanz de Galdeano et al., 2012).

2.4. Fault Slip Rates in the Granada Basin

In the Granada Basin, the transect between stations 6300 and 6400 crosses the Granada Fault System (Figure 2). Subtraction of the N060E components of these two stations yields a horizontal extension rate of 0.9 ± 0.3 mm/yr (Table 1 and Figure 3b). Once again, we compute fault slip rates assuming that all the deformation is accommodated by active faults. Therefore, our GNSS-derived data indicate a total cumulative slip rate ranging between 1.3 ± 0.6 and 1.8 ± 0.6 mm/yr for the Granada Fault System (assuming a mean dip of 45° and 60°, respectively).

Our GNSS-derived data indicate that the area located to the southwest of the Granada Basin is undergoing a horizontal shortening rate of 0.6 ± 0.4 mm/yr along the N060E direction. In this area, the main active structures are the Sierra Tejeda Anticline and the E–W Zafarraya Fault (Sanz de Galdeano et al., 2003, 2012). However, geological data indicate that the Zafarraya Fault presents oblique kinematics, including a normal component (Galindo-Zaldivar et al., 2003; Reicherter et al., 2003; Sanz de Galdeano et al., 2003, 2012). Therefore, further studies are necessary to elucidate the present kinematics of this significant active fault and its relationship with folding in a setting with shortening.

2.5. Comparison Between Short- and Long-Term Slip Rates

As discussed above, from our GNSS-derived data, we calculate the short-term slip rates of several active faults of the Central Betic Cordillera assuming that all the horizontal deformation is accommodated by active faults. In this section, we compare our short-term slip rates and geological long-term slip rates that were previously reported.

In the NE sector of the Guadix-Baza Basin, the short-term slip rates that we obtained for the Baza Fault range between 0.9 ± 0.3 and 1.3 ± 0.4 mm/yr (assuming fault dips of 45° and 60°, respectively). These values are higher

than previously reported long-term slip rates, varying between 0.2 and 0.7 mm/yr (using an Upper Tortonian stratigraphic marker and a 250–600 ky old geomorphic marker, assuming fault dips of 45° and 60°, respectively) (Alfaro et al., 2008; García-Tortosa et al., 2011) (see the relevant discussion in Alfaro et al. (2021)).

In the SW sector of the Guadix-Baza Basin, we estimated that the fault slip rate of the Solana del Zamborino Fault is approximately 0.1 mm/yr, although this value is just a rough approximation because of the very low signal-to-noise ratio, as we discussed above. Previously reported long-term fault slip rates for this fault range between 0.1 and 0.3 mm/yr (using a 250–600 ky old geomorphic marker and assuming fault dips of 45° and 60°, respectively) (García-Tortosa et al., 2011; Sanz de Galdeano et al., 2012). Therefore, in the case of the Solana del Zamborino Fault, both the long- and short-term slip rates are within the same range.

In the NW part of the Granada Basin, our GNSS-derived data indicate total cumulative slip rates of 1.3 ± 0.6 to 1.8 ± 0.6 mm/yr for the Granada Fault System (assuming a mean fault dips of 45° and 60°, respectively). The long-term slip rate calculated for this fault system using a Late Tortonian marker ranges between 0.2 and 0.6 mm/yr (Gil et al., 2002). Thus, once again, the short-term slip rate of the Granada Fault System that we calculated from our GNSS analysis is faster than the geological long-term slip rates reported in previous works.

Consequently, our GNSS-derived data yield short-term slip rates for the active faults of the Central Betic Cordillera that are higher than geologically computed long-term slip rates (except for the Solana del Zamborino Fault, where our GNSS data present a very low signal-to-noise ratio). Such differences between geodetic and geologic slip rates are not rare (e.g., Cowgill et al., 2009; Oskin et al., 2008). A possible explanation for these differences is a viscoelastic perturbation of the steady-state crustal motion that occurred after a major seismic event (Chuang & Johnson, 2011; Nur & Mavko, 1974; Savage & Prescott, 1978; Tong et al., 2014). In the case of the Central Betic Cordillera, no major earthquakes have taken place in the last 500 years (Instituto Geográfico Nacional, 2022); thus, we suggest that it is unlikely that a viscoelastic relaxation is still ongoing. Alternatively, discrepancies between short- and long-term slip rates could be the consequence of fault slip rate variations in time and/or space (McClymont et al., 2009; Nicol et al., 2010; Schlagenhauf et al., 2010, among many others). These rate variations influence the tectonic loading of faults and thus potentially trigger earthquake clusters (Oskin et al., 2008). This could be the case for the Granada Fault System, where subsequent earthquake swarm activity developed in January 2021 (Instituto Geográfico Nacional, 2022; Madarieta-Txurruka et al., 2021).

Otherwise, the discrepancy between the proposed geological and geodetic fault slip rates in the Central Betic Cordillera could also be explained assuming that part of the quantified extension rate is distributed in the rock volume between the major faults. Usually, most deformation in active areas is assumed to accumulate along the mapped major faults. However, a significant fraction of deformation could also be accommodated as internal deformation at the scale of observation. Moreover, there are several examples of recent earthquakes that occurred on previously unknown faults, such as the 2011 Darfield-Chistchurch event (England & Jackson, 2011). We consider the existence of unknown major faults in our study area very unlikely because the surface expression of these active normal faults is very clear in the study region, but we cannot rule out this hypothesis. In fact, this could be the case in the southwest Granada Basin, where the extension between sites 6100 and 6200 is 0.4 ± 0.3 mm/yr, without any significant main fault. Therefore, in our case, long-term geological slip rates are related to an active structure, as they compute the offset of a marker, that is, long-term slip rates account only for deformation related to one single fault. In contrast, short-term geodetic slip rates account for deformation along a transect and thus include displacement of active faults but also minor structures and hypothetical unknown faults.

2.6. Extension Partitioning in the Central Betic Cordillera

To analyze strain partitioning in the study region, we also subtracted the N060E component of different stations (Figure 5). We quantified extension in the Guadix-Baza Basin by comparing the N060E component of the residual velocity vectors of stations 5600, 5500, and 6400 (Table 1 and Figure 3b). This comparison indicates that the Guadix-Baza Basin is presently undergoing general ENE–WSW extension, as the N060 E components at these stations gradually increase from east to west. However, the distribution of this extension is highly heterogeneous (Figure 5). If we subtract the N060E component of stations 5600-5500 and 5500–6400, we obtain extension rates of 0.7 ± 0.4 and 0.1 ± 0.4 mm/yr, respectively. Consequently, GNSS-derived data indicate that most of the extension in the Guadix-Baza Basin is accommodated in the NE part of the basin (Figure 3b).

To analyze deformation in the region located between the Guadix-Baza and Granada Basins, we compared the N060 E component of the residual velocity vectors of stations 6400 and 6300 (Table 1 and Figure 3b). In that
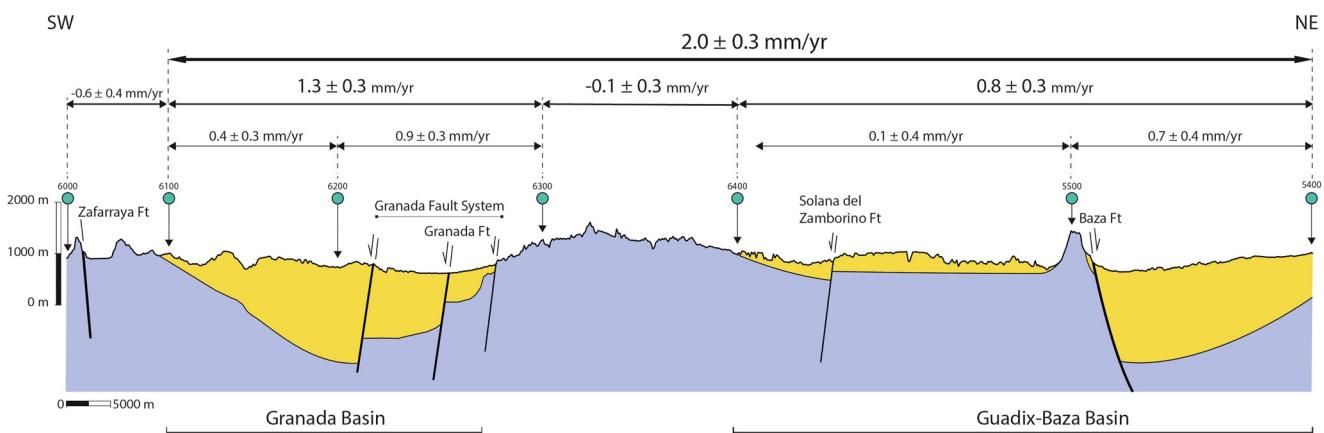
Figure 5. Simplified geological profile along the study GNSS profile (green dots are GNSS stations). Deformation rates are computed by subtracting the N060 component of different stations. The computed deformation rates show the heterogeneous partitioning of deformation along the Central Betic Cordillera. Note the exaggerated vertical scale.

case, the subtraction of these components yields an extension rate of -0.1 ± 0.3 mm/yr (Figure 5). This value is not statistically significant (at the 95% confidence level) because of the low signal-to-noise ratio. Thus, we interpreted that deformation in this area is very low (under the confidence level of our analysis).

Extension in the Granada Basin can be analyzed by comparing the N060E components of stations 6300, 6200, and 6100 (Table 1, Figure 3b). The subtraction of the components of stations 6300 and 6100 yields a total extension rate of 1.3 ± 0.3 mm/yr for the Granada Basin. Once again, this extension is heterogeneously distributed along the basin (Figure 5). The transect comprising stations 6300-6200 accommodates most of this extension (0.9 ± 0.3 mm/yr), while the southwestern part of the basin accommodates 0.4 ± 0.3 mm/yr (stations 6200-6100).

Finally, the comparison of the N060E components of stations 6100 and 6000 yields an extension rate of -0.6 ± 0.4 mm/yr. This value indicates that this area is undergoing shortening along the N060E direction, as discussed above.

The above exposed GNSS-derived velocity field indicates that the 2.0 ± 0.3 mm/yr overall extension within the Central Betic Cordillera is heterogeneous. The analysis of the N060E components of the velocity vectors (Figure 3b) shows that NE–SW extension is localized in two main areas characterized by thick sedimentary infill: the Guadix-Baza Basin and the Granada Basin (Figure 5). These two extensional areas are separated by a zone with no significant deformation (at the resolution of our data) characterized by extensive outcrops of basement rocks (Figure 2). The eastern borders of the two extensional areas are the normal Baza Fault and the Granada Fault System (Figure 2). Consequently, the active Central Betic Cordillera can be described as two half-grabens (the Guadix-Baza and Granada Basins) separated by a horst with no significant internal deformation (Figure 5).

Moreover, extension partitioning within the Guadix-Baza and Granada Basins is also heterogeneous. The Guadix-Baza Basin is undergoing a total NE–SW extension of 0.8 ± 0.3 mm/yr. This extension is mainly concentrated in the NE sector (0.7 ± 0.4 mm/yr of extension rate between stations 5600-5500) and is much lower in the SW sector of the basin (0.1 ± 0.4 mm/yr of extension rate between stations 5500–6400) (Figure 5).

Similarly, extension partitioning in the Granada Basin is also heterogeneous. The total NE–SW extension in the Granada Basin is 1.3 ± 0.3 mm/yr (Figure 5). Most of this extension is concentrated in the NE sector of the basin (0.9 ± 0.3 mm/yr of extension rate between stations 6300 and 6200). The SW sector of the basin accommodates 0.4 ± 0.3 mm/yr of extension (between stations 6200 and 6100). Previously reported cGNSS-derived data indicate a higher extension rate (1.8 ± 0.7 mm/yr) for the NE Granada Basin (Galindo-Zaldivar et al., 2015). However, this higher extension rate is based on the velocity vector of one station (GRA1) located at the top of a building based on the sedimentary infill of the Granada Basin. This sedimentary infill is undergoing localized ground surface movements related to groundwater addition and subtraction (Mateos et al., 2017; Notti et al., 2016; Sousa et al., 2010). Therefore, we consider that precautions should be taken when using station GRA1 for active tectonics studies.

Furthermore, our data permit a detailed analysis of the strain distribution between the faults forming the Granada Fault System. Two leveling profiles carried out along the Granada Fault (one of the active faults of the fault system) yielded a horizontal extension ranging between 0.2 ± 0.1 and 0.6 ± 0.3 mm/yr (assuming a mean fault dip of 60°, Madarieta-Txurruka et al., 2021). Consequently, the comparison between these values and our GNSS-derived extension rates indicates that the rest of the active faults of the Granada Fault System accommodate ≈0.3–0.7 mm/yr of extension. No outcrops of active faults have been previously identified in the SW part of the Granada Basin (Figure 2). However, our GNSS-derived data indicate that this area is undergoing extension (0.4 ± 0.3 mm/yr between stations 6200 and 6100) (see below).

2.7. Insights Into Structural Style in the Central Betic Cordillera

As we already mentioned, our GNSS-derived data indicate that the SW part of the Granada Basin is undergoing extension (0.4 ± 0.3 mm/yr between stations 6200 and 6100) yr (Table 1, Figures 3b and 4). Active deformation in this part of the basin is further supported by the shallow (less than 15 km) (Morales et al., 1997) instrumental seismicity. However, no outcropping active fault has been previously identified in this area (Figure 6).

Madarieta-Txurruka et al. (2021) postulate that the outcropping faults of the Granada Fault System appear to lie downwards in a SW-dipping low-angle normal fault (likely the Mecina Detachment Zone). This fault coalescence was also proposed for other high-angle faults offsetting the basement rocks to the southeast of the Granada Basin (Galindo-Zaldívar et al., 1996). Low-angle detachment zones in the Betic Cordillera developed during the Lower Miocene, that is, prior to the formation of the Granada Fault System (Crespo-Blanc et al., 1994; Jabaloy et al., 1992). Therefore, the hypothetical coalescence of the Granada Fault System with a low-angle detachment zone would imply an interaction between newly formed and preexisting intrabasement faults. Interactions between intrabasement structures and newly formed normal faults have been widely reported in the literature (Fraser & Gawthorpe, 1990; Morley et al., 2004; Phillips et al., 2016; Ring, 1994; Salomon et al., 2015). The exact manner in which previous extensional structures influence later normal faults was observed by Phillips et al. (2016) in offshore southern Norway. In this area, intrabasement Devonian extensional shear zones were reactivated by high-angle Carboniferous-early Permian normal faults (Ziegler, 1992). Phillips et al. (2016) observed three different styles of interaction between newly formed normal faults and preexisting intrabasement low-angle faults (Figure 6): (a) Merging faults, located in the hanging wall of intrabasement faults and striking subparallel to them. Merging faults coalesce with the margins of preexisting basement faults at depth. (b) Exploiting faults, dipping and striking subparallel to intrabasement faults. Under this type of interaction, reactivation occurs by exploiting internal weak zones within basement faults. (c) Cross-cutting faults dipping and striking obliquely to intrabasement faults. In that case, newly formed faults are neither geometrically nor kinematically linked with preexisting basement faults.

Faults of the Granada Fault System merge with a low-angle detachment in map view, suggesting an analogous interaction at depth. According to Galindo-Zaldívar et al., 1996 and Madarieta-Txurruka et al. (2021), this structure is the Mecina Detachment Zone (Figure 6). We interpret the Granada Fault System as a merging fault (in the sense of Phillips et al., 2016). Therefore, these two structures would be geometrically linked. In that case, a kinematic link is also expected. This kinematic link is also supported by our data, as they indicate that the Granada Fault System accommodates an extension rate of 0.9 ± 0.3 mm/yr (stations 6300-6200). This value is compatible with the extension rate derived from cGNSS data for the Mecina Detachment (1.1 ± 0.3 mm/yr, Galindo-Zaldivar et al., 2015), while the SW sector of the basin accommodates 0.4 ± 0.3 mm/yr (stations 6200-6100). These two values are compatible with such a kinematic link, accounting for the computed errors.

Seismic reflection data suggest that the Baza Fault, the main active structure in this area, becomes listric with depth (Haberland et al., 2017), but no further constraints of the deep structure in this area are available. In map view, the Baza Fault is geometrically and kinematically linked to the strike-slip Galera Fault (Figure 2) (Alfaro et al., 2021; Medina-Cascales et al., 2021), but no interaction with preexisting intrabasement faults is observed.

To provide a wider geodynamic interpretation of the Central Betic Cordillera encompassing available geological and geophysical data as well as our geodetic results, we compare our proposed structural model with the Eastern Basin and Range in the USA. The Eastern Basin and Range is a seismically active extensional region characterized by alternating mountain ranges and sedimentary basins (Smith & Sbar, 1974; Velasco et al., 2010). The present overall extension along the Eastern Basin and Range reaches up to 3 mm/yr over 350 km (Bennett et al., 2003; Friedrich et al., 2003; Niemi et al., 2004). Seismic reflection data (Velasco et al., 2010) show that the eastern end
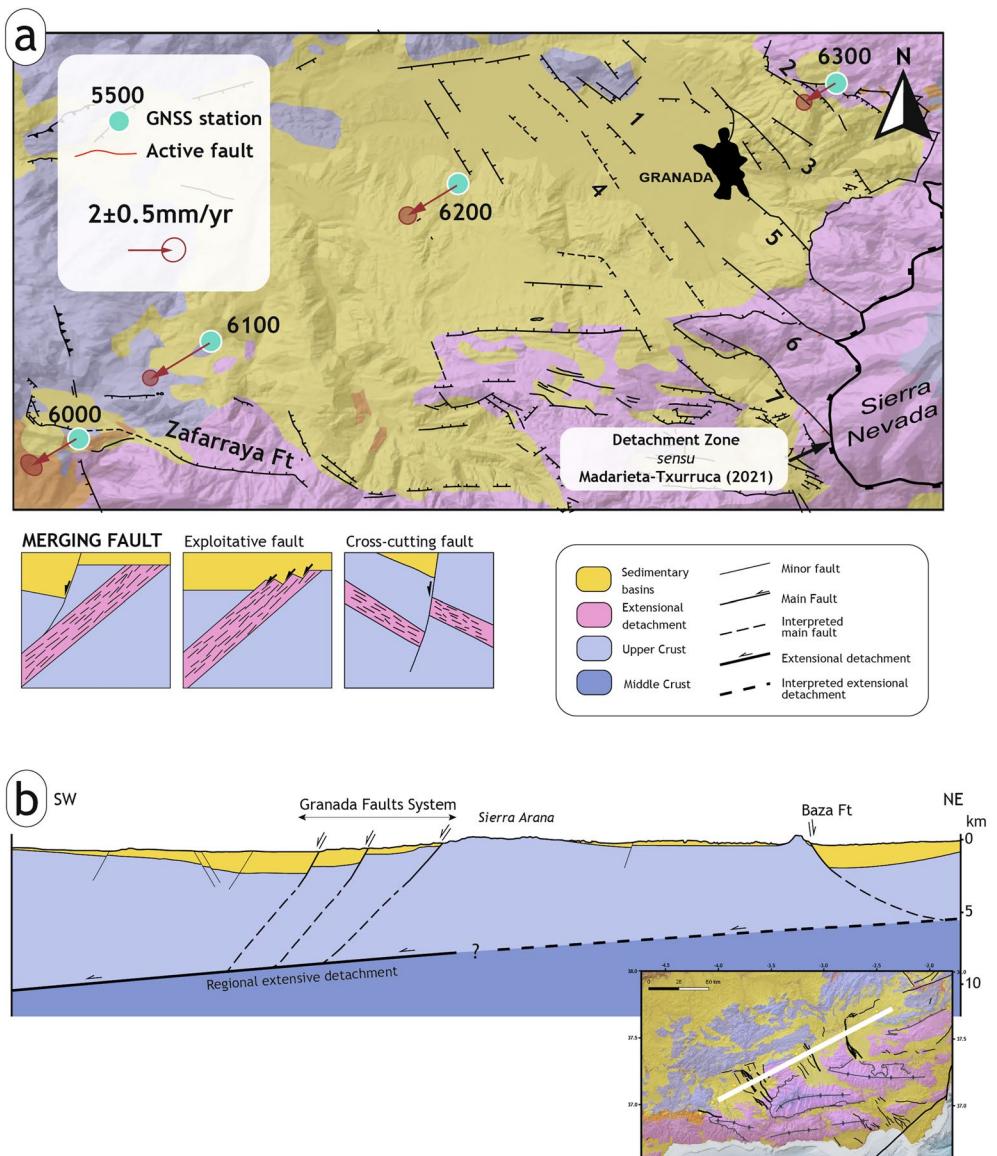
Figure 6. Extensional system linking low- and high-angle faults. (a) Map of the Granada Basin showing the main active faults (after Madarieta-Txurruka et al., 2021). According to Madarieta-Txurruka et al. (2021), the Granada Fault System (faults 2, 3, 5, and 7) merges in map view with the low-angle Mecina Detachment Zone. Three different styles of interaction between newly formed normal faults and preexisting intrabasement low-angle faults are shown (modified from Phillips et al. (2016)). The interaction of the Granada Fault System corresponds to style I (merging faults). (b) Cross-section illustrating the hypothesis that the low-angle detachment zone soling the Granada Fault System could also be a regional detachment. White line in inset show the approximate position of the cross section. Legend as in Figure 3.

of the Eastern Basin and Range consists of two major antithetic normal faults (Wasatch and Gunninson Faults), creating half-grabens where Cenozoic and Quaternary sediments were deposited (Figure 6). The Wasatch and Gunninson normal faults bound a basement horst (San Pitch Mountains) (Figure 6), and both of these active faults coalesce at depth with a low-angle preexisting detachment zone (Constenius et al., 2003; Velasco et al., 2010). This low-angle surface is interpreted as a regional extensive detachment linking the most active normal faults cropping out at depth in the Eastern Basin and Range (Velasco et al., 2010).

Further studies are necessary to elucidate the subsurface geometry of the Central Betic Cordillera. However, the proposed extension rate and surface structural style of the Central Betic Cordillera resemble those of the eastern end of the Eastern Basin and Range. Despite significant differences between our study area and the Basin and Range, such as the heat flow and areal amplitude of the extensional area (Soto et al., 2008), the observed

similarities could suggest an analogous subsurface structure. If this is the case, the low-angle detachment zone soling the Granada Fault System (Madarieta-Txurruka et al., 2021) could also be a regional extensive detachment. Therefore, other normal faults in our study area, including the Baza Fault, could hypothetically also coalesce at depth in this low-angle detachment (Figure 6). Our GNSS-derived data are compatible with this hypothesis, as the overall horizontal velocity field for the Central Betic Cordillera shows a southwest motion of all stations with a southwestward increase in the N060 E components (Figure 3b). In any case, we would like to emphasize that additional research is required to clarify this highly hypothetical subsurface structure of the Central Betic Cordillera.

2.8. Geodynamic Implications

The Betic Cordillera is a collisional orogen that is presently dominated by the convergence between the Nubian and Eurasian plates (DeMets et al., 1994; McClusky et al., 2003; Nocquet, 2012; Nocquet & Calais, 2003; Pérez-Peña et al., 2010; Serpelloni et al., 2007; Stich et al., 2006). Because of this convergence, the Western and Eastern Betic Cordillera are undergoing shortening and transpression, respectively (Borque et al., 2019; Echeverria et al., 2013, 2015; Gonzalez-Castillo et al., 2015) (Figure 1). Within this convergent geodynamic framework, our GNSS data indicate that the Central Betic Cordillera accommodates 2.0 ± 0.3 mm/yr of overall NE–SW extension (Figure 5). Moreover, our results indicate that the Central Betic Cordillera consists of a horst bounded by two half-grabens, where sedimentary basins developed from the Upper Miocene onwards (Figure 5).

Despite being an extensional domain, the Central Betic Cordillera is characterized by the highest topography of the entire mountain range (Figures 1 and 6). Subsurface data also indicate that the Central Betic Cordillera presents an overthickened crust (~35 km) as a consequence of duplex formation, folding and thrusting related to the underthrusting of the Iberian basement beneath the Betic orogenic wedge (Galindo-Zaldívar et al., 1997).

Therefore, the upper crust of the Central Betic Cordillera is an elevated area undergoing extension, with extensional basins and characterized by an overthickened crust (Figure 7). Analogous geodynamic situations have been described in other convergent settings. For instance, Crete in the eastern Mediterranean is also an extensional region within a general convergent geodynamic cadre related to the Nubia-Eurasia convergence. Crete is characterized by thick crust (~40 km) (Gudmundsson & Sambridge, 1998; Meier et al., 2004) and relatively high topography. Extension in Crete in the upper part of the crust has been interpreted as the consequence of regional uplift related to gravitational instability of the overthickened crust (Gallen et al., 2014). In Crete, the overthickened crust is the result of thrusting and folding associated with the underplating of the African oceanic crust under Eurasia. Therefore, according to the abovementioned similarities, we postulate that an analogous process could also play a role in the active extension observed in the Central Betic Cordillera (Figure 7). That is, we hypothesize that part of the 2.0 ± 0.3 mm/yr of overall NE–SW extension indicated by our GNSS data for the Central Betic Cordillera may be the result of upper crustal extension derived from gravitational instability because of the underlying overthickened crust. Notably, this gravitational extension is compatible with any of the other geodynamic processes invoked by previous authors, such as slab rollback related to active subduction located further west (e.g., Galindo-Zaldivar et al., 2015; González-Castillo et al., 2015; Gustcher et al., 2002), deep-seated delamination processes (e.g., Baratin et al., 2016; Fadil et al., 2006; Pérouse et al., 2010; Petit et al., 2015; Soto et al., 2008; among others) or slab drag (Spakman et al., 2018).

3. Conclusions

The GNSS data discussed here represent a significant advance in the characterization of deformation partitioning in the westernmost part of the peri-Mediterranean orogenic belt. We quantitatively characterize deformation in the Central Betic Cordillera, an extensional area within this shortening-dominated collisional orogen. Our data indicate that the total extension in this area is 2.0 ± 0.3 mm/yr. In addition, we show that this deformation is highly heterogeneous. We identify two areas of extension, the Guadix-Baza Basin to the east (accommodating 0.8 ± 0.3 mm/yr) and the Granada Basin to the west (accommodating 1.3 ± 0.3 mm/yr). These two extensional areas are separated by a zone in which no significant deformation occurs. Moreover, deformation partitioning within the two mentioned extensional areas is also heterogeneous. Therefore, we describe the analyzed transect of the Central Betic Cordillera as two half-grabens (the Guadix-Baza and Granada Basins) undergoing extension separated by a horst with no significant internal deformation, similar to that observed in the Basin and Range.

Our GNSS data widen the knowledge of fault slip rates of active faults in the Central Betic Cordillera. We present, for the first time, short-term slip rates for two of these faults. We obtained a fault slip rate of 0.1 ± 0.4 mm/yr for the Solana del Zamborino Fault. In the case of the Granada Fault System, we obtained a fault slip rate of
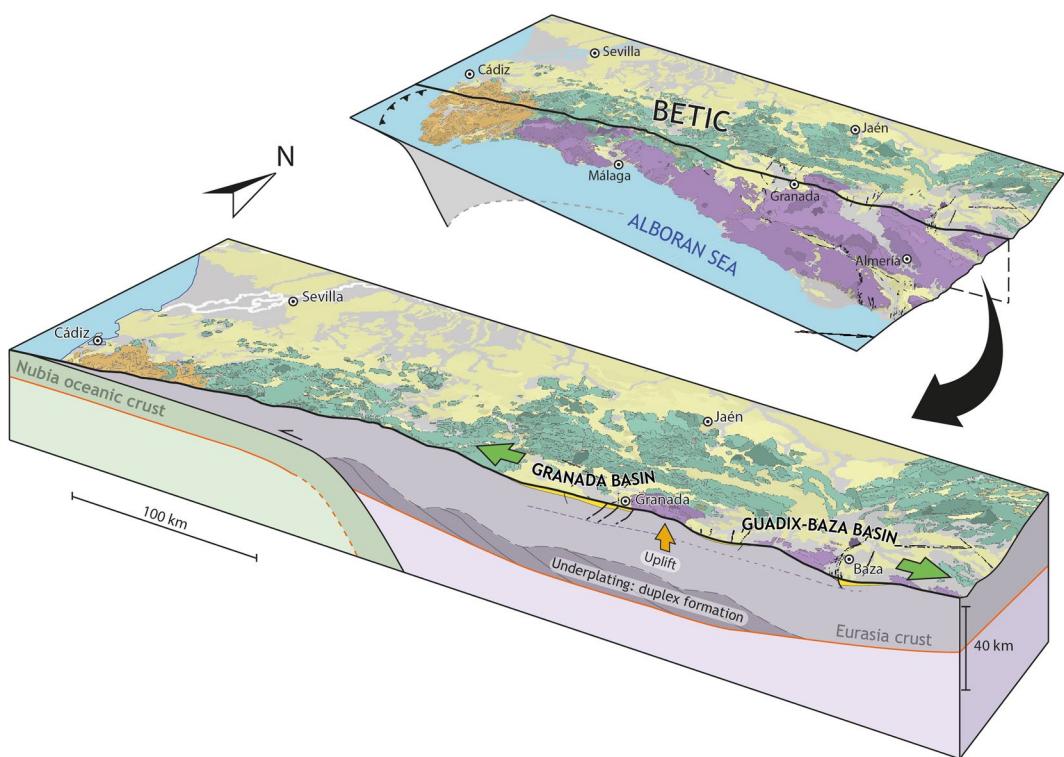
Figure 7. Southwest–northeast oriented 3D view of the Betic Cordillera showing the regional topography and schematic crustal structure. The Central Betic Cordillera presents the highest topographic relief and the thickest crust (related to underplating) of the orogen. Our results indicate that the Central Betic Cordillera is an extensional area (green arrows indicate regional extension). We postulate that this extension could be partially related to an extensional collapse driven by the regional uplift (orange arrow) produced by underplating.

0.9 ± 0.3 mm/yr. These new data represent a significant advance for the seismic characterization of the Central Betic Cordillera, as they will be the input for future seismic hazard assessments. This is especially relevant for the Granada Fault System, as this seismogenic structure is located in a highly populated area.

We also postulate that the outcropping high-angle normal faults accommodating extension may sole downwards in a regional extensional detachment. Furthermore, we discuss that, according to the interaction between the hypothetical low-angle detachment and the Granada Fault System, the latter could be considered a merging fault (sensu Phillips et al., 2016).

The results discussed here shed light on the deformation partitioning along an extensional domain located in a convergence-dominated setting. We hypothesize that part of the present extension could be the result of gravitational instability related to an overthickened crust. This hypothesis opens a new discussion about the tectonic process presently active in the western Mediterranean region.

Data Availability Statement

The RINEX files with the data used for computing the crustal velocity field in the study are available with CC BY 4.0 license at Mendeley Data (Martin-Rojas, 2022). Data processing was performed by Precise Point Positioning using GipsyX software (Bertiger et al., 2020b).

References

Aktug, B., Nocquet, J. M., Cingöz, A., Parsons, B., Erkan, Y., England, P., et al. (2009). Deformation of western Turkey from a combination of permanent and campaign GPS data: Limits to block-like behavior. *Journal of Geophysical Research*, *114*(B10), B10404. https://doi.org/10.1029/2008JB006000

Alfaro, P., Delgado, J., Galdeano, C. S., Galindo-Zaldívar, J., García-Tortosa, F. J., López-Garrido, A. C., et al. (2008). The Baza Fault: A major active extensional fault in the central Betic Cordillera (south Spain). *International Journal of Earth Sciences: Geologische Rundschau*, *97*(6), 1353–1365. https://doi.org/10.1007/s00531-007-0213-z

Alfaro, P., Sánchez-Alzola, A., Martin-Rojas, I., García-Tortosa, F. J., Galindo-Zaldívar, J., Avilés, M., et al. (2021). Geodetic fault slip rates on active faults in the Baza sub-Basin (SE Spain): Insights for seismic hazard assessment. *Journal of Geodynamics*, *144*, 101815. https://doi.org/10.1016/j.jog.2021.101815

Alfaro, P., Sanz de Galdeano Equiza, C., Garrido, L. A. C., Galindo Zaldívar, J., Alfaro, P., & Jabaloy Sánchez, A. (2001). Evidence for the activity and paleoseismicity of the Padul fault (Betic Cordillera, southern Spain). *Acta Geologica Hispanica*, *36*(3–4), 283–295.

Altamimi, Z., Métivier, L., Rebischung, P., Rouby, H., & Collilieux, X. (2017). ITRF2014 plate motion model. *Geophysical Journal International*, *209*(3), 1906–1912. https://doi.org/10.1093/gji/ggx136

Armijo, R., Meyer, B., Hubert, A., & Barka, A. (1999). Westward propagation of the North Anatolian fault into the northern Aegean: Timing and kinematics. *Geology*, *27*(3), 267–270. https://doi.org/10.1130/0091-7613(1999)0272.3.CO;2

Azañón, J. M., Azor, A., Booth-Rea, G., & Torcal, F. (2004). Small-scale faulting, topographic steps and seismic ruptures in the Alhambra (Granada, southeast Spain. *Journal of Quaternary Science*, *19*(3), 219–227. https://doi.org/10.1002/jqs.838

Baratin, L., Mazzotti, S., Chéry, J., Vernant, P., Tahayt, A., & Mourabit, T. (2016). Incipient mantle delamination, active tectonics and crustal thickening in Northern Morocco: Insights from gravity data and numerical modeling. *Earth and Planetary Science Letters*, *454*, 113–120. https://doi.org/10.1016/j.epsl.2016.08.041

Bennett, R. A., Wernicke, B. P., Niemi, N. A., Friedrich, A. M., & Davis, J. L. (2003). Contemporary strain rates in the northern Basin and Range province from GPS data. *Tectonics*, *22*(2), 1008. https://doi.org/10.1029/2001TC001355

Bertiger, W., Bar-Sever, Y., Dorsey, A., Haines, B., Harvey, N., Hemberger, D., et al. (2020a). GipsyX: 2022-08-23 release (Version 2.1) [Software]. *Jet Propulsion Laboratory*.

Bertiger, W., Bar-Sever, Y., Dorsey, A., Haines, B., Harvey, N., Hemberger, D., et al. (2020b). GipsyX/RTGx, a new tool set for space geodetic operations and research. *Advances in Space Research*, *66*(3), 469–489. https://doi.org/10.1016/j.asr.2020.04.015

Billi, A., Faccenna, C., Bellier, O., Minelli, L., Neri, G., Piromallo, C., et al. (2011). Recent tectonic reorganization of the Nubia-Eurasia convergent boundary heading for the closure of the Western Mediterranean. *Bulletin de la Societe Geologique de France*, *182*(4), 279–303. https://doi.org/10.2113/gssgfbull.182.4.279

Borque, M. J., Sánchez-Alzola, A., Martin-Rojas, I., Alfaro, P., Molina, S., Rosa-Cintas, S., et al. (2019). How much Nubia-Eurasia convergence is accommodated by the NE end of the eastern Betic shear zone (SE Spain)? Constraints from GPS velocities. *Tectonics*, *38*(5), 1824–1839. https://doi.org/10.1029/2018TC004970

Bousquet, J. (1979). Quaternary strike-slip faults in southeastern Spain. *Tectonophysics*, *52*(1), 277–286. https://doi.org/10.1016/0040-1951(79)90232-4

Calvache, M. L., Viseras, C., & Ferndacute;ez, J. (1997). Controls on fan development—Evidence from fan morphometry and sedimentology; Sierra Nevada, SE Spain. *Geomorphology*, *21*(1), 69–84. https://doi.org/10.1016/S0169-555X(97)00035-4

Castro, J., Martin-Rojas, I., Medina-Cascales, I., García-Tortosa, F. J., Alfaro, P., & Insua-Arévalo, J. M. (2018). Active faulting in the central Betic Cordillera (Spain): Palaeoseismological constraint of the surface-rupturing history of the Baza Fault (Central Betic Cordillera, Iberian Peninsula). *Tectonophysics*, *736*, 15–30. https://doi.org/10.1016/j.tecto.2018.04.010

Chuang, R. Y., & Johnson, K. M. (2011). *Reconciling geologic and geodetic model fault slip-rate discrepancies in Southern California: Consideration of nonsteady mantle flow and lower crustal fault creep*. The Geological Society of America. https://doi.org/10.1130/G32120.1

Constenius, K., Esser, R., & Layer, P. (2003). Extensional collapse of the Charleston-Nebo Salient and its relationship to space–time variations in Cordilleran orogenic belt tectonism and continental stratigraphy. In R. Raynolds & R. Flores (Eds.), *Cenozoic systems of the Rocky Mountains Region*. Rocky Mountain SEPM.

Coppier, G., Griveaud, P., de Larouziere, F., Montenat, C., & Ott d'Estevou, P. (1989). Example of Neogene tectonic indentation in the Eastern Betic Cordilleras: The arc of Aguilas (Southeastern Spain). *Geodinamica Acta*, *3*(1), 37–51. https://doi.org/10.1080/09853111.1989.11105173

Cowgill, E., Gold, R. D., Xuanhua, C., Xiaofeng, W. X., Arrowsmith, R., Southon, J. R., et al. (2009). Low Quaternary slip rate reconciles geodetic and geologic rates along the Altyn Tagh Fault, northwestern Tibet. *Geology*, *37*(7), 647–650. https://doi.org/10.1130/G25623A.1

Crespo-Blanc, A., Orozco, M., & Garcia-Dueñas, V. (1994). Extension versus compression during the Miocene tectonic evolution of the Betic chain. Late folding of normal fault systems. *Tectonics*, *13*(1), 78–88. https://doi.org/10.1029/93TC02231

d'Acremont, E., Lafosse, M., Rabaute, A., Teurquety, G., Do Couto, D., & Ercilla, G. (2020). Polyphase tectonic evolution of fore-arc basin related to STEP fault as revealed by seismic reflection data from the Alboran Sea (W-Mediterranean). *Tectonics*, *39*(3), e2019TC005885. https://doi.org/10.1029/2019TC005885

De Larouziere, F. D., Montenat, C., Ott D'Estevou, P., & Griveaud, P. (1987). Evolution simultanée de bassins néogènes en compression et en extension dans un couloir de décrochement: Hinojar et Mazarron (Sud-Est de l'Espagne). *Bulletin des Centres de Recherches Exploration-Production Elf-Aquitaine*, *11*(1), 23–38.

DeMets, C., Gordon, R. G., Argus, D. F., & Stein, S. (1994). Effect of recent revisions to the geomagnetic reversal time scale on estimates of current plate motions. *Geophysical Research Letters*, *21*(20), 2191–2194. https://doi.org/10.1029/94GL02118

Dewey, J. F., Helman, M. L., Knott, S. D., Turco, E., & Hutton, D. H. W. (1989). Kinematics of the Western Mediterranean. *Geological Society - Special Publications*, *45*(1), 265–283. https://doi.org/10.1144/GSL.SP.1989.045.01.15

Echeverria, A., Khazaradze, G., Asensio, E., Gárate, J., Dávila, J. M., & Suriñach, E. (2013). Crustal deformation in eastern Betics from CuaTeNeo GPS network. *Tectonophysics*, *608*, 600–612. https://doi.org/10.1016/j.tecto.2013.08.020

Echeverria, A., Khazaradze, G., Asensio, E., & Masana, E. (2015). Geodetic evidence for continuing tectonic activity of the Carboneras fault (SE Spain). *Tectonophysics*, *663*, 302–309. https://doi.org/10.1016/j.tecto.2015.08.009

England, P., & Jackson, J. (2011). Uncharted seismic risk. *Nature Geoscience*, *4*(6), 348–349. https://doi.org/10.1038/ngeo1168

Estevez, A., & Sanz de Galdeano, C. (1983). Néotectonique du secteur central des Chaînes Bétiques (Bassin du Guadix-Baza et de Grenade)./ (Neotectonic in the central area of the Betic Cordilleras). *Revue de Géologie Dynamique et de Géographie Physique*. Retrieved from https://search.proquest.com/docview/1307727036

Estrada, F., Galindo-Zaldívar, J., Vázquez, J. T., Ercilla, G., D'Acremont, E., Alonso, B., & Gorini, C. (2018). Tectonic indentation in the central Alboran Sea (westernmost Mediterranean). *Terra Nova*, *30*(1), 24–33. https://doi.org/10.1111/ter.12304

Faccenna, C., Becker, T. W., Auer, L., Billi, A., Boschi, L., Brun, J. P., et al. (2014). Mantle dynamics in the Mediterranean. *Reviews of Geophysics*, *52*(3), 283–332. https://doi.org/10.1002/2013RG000444

Fadil, A., Vernant, P., McClusky, S., Reilinger, R., Gomez, F., Ben Sari, D., et al. (2006). Active tectonics of the western Mediterranean; geodetic evidence for rollback of a delaminated subcontinental lithospheric slab beneath the Rif Mountains, Morocco. *Geology*, *34*(7), 529–532. https://doi.org/10.1130/G22291.1

Fernández-Ibáñez, F., Pérez-Peña, J. V., Azor, A., Soto, J. I., & Azañón, J. M. (2010). Normal faulting driven by denudational isostatic rebound. *Geology*, *38*(7), 643–646. https://doi.org/10.1130/g31059.1

Ford, M., Hemelsdaël, R., Mancini, M., & Palyvos, N. (2017). Rift migration and lateral propagation: Evolution of normal faults and sediment-routing systems of the western Corinth rift (Greece). *Geological Society - Special Publications*, *439*(1), 131–168. https://doi.org/10.1144/SP439.15

Ford, M., Williams, E. A., Malartre, F., & Popescu, S. (2007). Stratigraphic architecture, sedimentology and structure of the vouraikos Gilbert-type Fan Delta, Gulf of Corinth, Greece. https://doi.org/10.1002/9781444304411.ch4

Fraser, A. J., & Gawthorpe, R. L. (1990). Tectono-stratigraphic development and hydrocarbon habitat of the Carboniferous in northern England. *Geological Society - Special Publications*, *55*(1), 49–86. https://doi.org/10.1144/GSL.SP.1990.055.01.03

Friedrich, A. M., Wernicke, B. P., Niemi, N. A., Bennett, R. A., & Davis, J. L. (2003). Comparison of geodetic and geologic data from the Wasatch region, Utah, and implications for the spectral character of Earth deformation at periods of 10 to 10 million years. *Journal of Geophysical Research*, *108*(B4). https://doi.org/10.1029/2001JB000682

Galindo-Zaldívar, J., Gil, A. J., Borque, M. J., González-Lodeiro, F., Jabaloy, A., & Marín-Lechado, C. (2003). Active faulting in the internal zones of the central Betic Cordilleras (SE, Spain). *Journal of Geodynamics*, *36*(1), 239–250. https://doi.org/10.1016/S0264-3707(03)00049-8

Galindo-Zaldívar, J., Gil, A. J., Sanz de Galdeano, C., Lacy, M. C., García-Armenteros, J. A., Ruano, P., et al. (2015). Active shallow extension in central and eastern Betic Cordillera from CGPS data. *Tectonophysics*, *663*, 290–301. https://doi.org/10.1016/j.tecto.2015.08.035

Galindo-Zaldívar, J., Gil, A. J., Tendero-Salmerón, V., Borque, M. J., Ercilla, G., González-Castillo, L., et al. (2022). The Campo de Dalias GNSS Network Unveils the interaction between roll-Back and indentation tectonics in the Gibraltar arc. *Sensors*, *22*(6), 2128. https://doi.org/10.3390/s22062128

Galindo-Zaldívar, J., & Jabaloy, A. (1989). Progressive extensional shear structures in a detachment contact in the Western Sierra Nevada (Betic Cordilleras, Spain)/(Structures progressives en cisaillement extensif dans un détachement à la partie occidentale de la Sierra Névada (Cordillères bétiques, Espagne).). *Geodinamica Acta*, *3*(1), 73–85. https://doi.org/10.1080/09853111.1989.11105175

Galindo-Zaldívar, J., Jabaloy, A., & González-Lodeiro, F. (1996). Reaction of the Mecina detachment in the Western sector of Sierra Nevada (Betic Cordilleras, SE Spain). *Comptes Rendus De L'Académie Des Sciences. Série II. Fascicule a, Sciences De La Terre Et Des Planètes*, *323*(7), 615–622.

Galindo-Zaldívar, J., Jabaloy, A., González-Lodeiro, F., & Aldaya, F. (1997). Crustal structure of the central sector of the Betic Cordillera (SE Spain). *Tectonics*, *16*(1), 18–37. https://doi.org/10.1029/96TC02359

Galindo-Zaldívar, J., Jabaloy, A., Serrano, I., Morales, J., González-Lodeiro, F., & Torcal, F. (1999). Recent and present-day stresses in the Granada Basin (Betic Cordilleras): Example of a late Miocene-present-day extensional basin in a convergent plate boundary. *Tectonics*, *18*(4), 686–702. https://doi.org/10.1029/1999TC900016

Gallen, S. F., Wegmann, K. W., Bohnenstiehl, D. R., Pazzaglia, F. J., Brandon, M. T., & Fassoulas, C. (2014). Active simultaneous uplift and margin-normal extension in a forearc high, Crete, Greece. *Earth and Planetary Science Letters*, *398*, 11–24. https://doi.org/10.1016/j.epsl.2014.04.038

García-Tortosa, F. J., Alfaro, P., Galindo-Zaldívar, J., Gibert, L., López-Garrido, A. C., Sanz de Galdeano, C., & Ureña, M. (2008). Geomorphologic evidence of the active Baza Fault (Betic Cordillera, South Spain). *Geomorphology*, *97*(3), 374–391. https://doi.org/10.1016/j.geomorph.2007.08.007

García-Tortosa, F. J., Alfaro, P., Sanz de Galdeano, C., & Galindo-Zaldívar, J. (2011). Glacis geometry as a geomorphic marker of recent tectonics: The Guadix–Baza basin (South Spain). *Geomorphology*, *125*(4), 517–529. https://doi.org/10.1016/j.geomorph.2010.10.021

Gawthorpe, R. L., Leeder, M. R., Kranis, H., Skourtsos, E., Andrews, J. E., Henstra, G. A., et al. (2018). Tectono-sedimentary evolution of the Plio-Pleistocene Corinth rift, Greece. *Basin Research*, *30*(3), 448–479. https://doi.org/10.1111/bre.12260

Gil, A. J., Galindo-Zaldívar, J., de Sanz Galdeano, C., Borque, M. J., Sánchez-Alzola, A., Martínez-Martos, M., & Alfaro, P. (2017). The Padul normal fault activity constrained by GPS data: Brittle extension orthogonal to folding in the central Betic Cordillera. *Tectonophysics*, *712–713*, 64–71. https://doi.org/10.1016/j.tecto.2017.05.008

Gil, A. J., Rodríguez-Caderot, G., Lacy, M. C., Ruiz, A. M., Sanz de Galdeano, C., & Alfaro, P. (2002). Establishment of a non-permanent GPS network to monitor the recent NE-SW deformation in the Granada Basin (Betic Cordillera, Southern Spain). *Studia Geophysica et Geodaetica*, *46*(3), 395–410. https://doi.org/10.1023/A:1019530716324

Gonzalez-Castillo, L., Galindo-Zaldivar, J., de Lacy, M. C., Borque, M. J., Martinez-Moreno, F. J., García-Armenteros, J. A., & Gil, A. J. (2015). Active rollback in the Gibraltar arc: Evidences from CGPS data in the Western Betic Cordillera. *Tectonophysics*, *663*, 310–321. https://doi.org/10.1016/j.tecto.2015.03.010

Gudmundsson, Ó., & Sambridge, M. (1998). A regionalized upper mantle (RUM) seismic model. *Journal of Geophysical Research*, *103*(B4), 7121–7136. https://doi.org/10.1029/97JB02488

Gutscher, M. A., Malod, J., Rehault, J. P., Contrucci, I., Klingelhoefer, F., Mendes-Victor, L., & Spakman, W. (2002). Evidence for active subduction beneath Gibraltar. *Geology*, *30*(12), 1071–1074. https://doi.org/10.1130/0091-7613(2002)030<1071:EFASBG>2.0.CO;2

Haberland, C., Gibert, L., Jurado, M. J., Stiller, M., Baumann-Wilke, M., Scott, G., & Mertz, D. F. (2017). Architecture and tectono-stratigraphic evolution of the intramontane Baza Basin (Bétics, SE-Spain): Constraints from seismic imaging. *Tectonophysics*, *709*, 69–84. https://doi.org/10.1016/j.tecto.2017.03.022

Herraiz, M., De Vicente, G., Lindo-Ñaupari, R., Giner, J., Simón, J. L., González-Casado, J. M., et al. (2000). The recent (upper Miocene to Quaternary) and present tectonic stress distributions in the Iberian Peninsula,. *Tectonics*, *19*(4), 762–786. https://doi.org/10.1029/2000TC900006

Instituto Geográfico Nacional. (2022). Catálogo de terremotos. Retrieved from https://www.ign.es/web/ign/portal/sis-catalogo-terremotos

Jabaloy, A., Galindo-Zaldívar, J., & González-Lodeiro, F. (1992). The Mecina extensional system: Its relation with the post-Aquitanian piggy-back Basins and the paleostresses evolution (Betic Cordilleras, Spain). *Geo-Marine Letters*, *12*(2–3), 96–103. https://doi.org/10.1007/BF02084918

Jabaloy, A., Galindo-Zaldívar, J., & González-Lodeiro, F. (1993). The Alpujárride-Nevado-Fibábride extensional shear zone, Betic Cordillera, SE Spain. *Journal of Structural Geology*, *15*(3), 555–569. https://doi.org/10.1016/0191-8141(93)90148-4

Jolivet, L., Baudin, T., Calassou, S., Chevrot, S., Ford, M., Issautier, B., et al. (2021). Geodynamic evolution of a wide plate boundary in the Western Mediterranean, near-field versus far-field interactions. *Bulletin de la Societe Geologique de France*, *192*, 48. https://doi.org/10.1051/bsgf/2021043

Jolivet, L., & Faccenna, C. (2000). Mediterranean extension and the Africa-Eurasia collision. *Tectonics*, *19*(6), 1095–1106. https://doi.org/10.1029/2000TC900018

Lhénaff, R. (1965). Néotectonique quaternaire sur le bord occidental de la Sierra Nevada (Province de Grenade, Espagne). *Revue de Geographie Physique et de Geologie Dynamique*, *7*(3), 205.

Lonergan, L., & White, N. (1997). Origin of the Betic-Rif mountain belt. *Tectonics*, *16*(3), 504–522. https://doi.org/10.1029/96TC03937

Lozano, L., Cantavella, J. V., Gaite, B., Ruiz-Barajas, S., Antón, R., & Barco, J. (2022). Seismic analysis of the 2020–2021 Santa Fe seismic sequence in the Granada Basin, Spain: Relocations and focal mechanisms. *Seismological Society of America*, *93*(6), 3246–3265. https://doi.org/10.1785/0220220097

Madarieta-Txurruka, A., Galindo-Zaldívar, J., González-Castillo, L., Peláez, J. A., Ruiz-Armenteros, A. M., Henares, J., et al. (2021). High- and low-angle normal fault activity in a Collisional Orogen: The Northeastern Granada Basin (Betic Cordillera). *Tectonics*, *40*(7). https://doi.org/10.1029/2021TC006715

Madarieta-Txurruka, A., González-Castillo, L., Peláez, J. A., Catalán, M., Henares, J., Gil, A. J., et al. (2022). The role of faults as barriers in confined seismic sequences: 2021 seismicity in the Granada Basin (Betic Cordillera). *Tectonics*, *41*(9). https://doi.org/10.1029/2022TC007481

Mancilla, F. L., Booth-Rea, G., Stich, D., Pérez-Peña, J. V., Morales, J., Azañón, J. M., et al. (2015). Slab rupture and delamination under the Betics and Rif constrained from receiver functions. *Tectonophysics*, *663*, 225–237. https://doi.org/10.1016/j.tecto.2015.06.028

Mancilla, F. D. L., Stich, D., Berrocoso, M., Martín, R., Morales, J., Fernandez-Ros, A., et al. (2013). Delamination in the Betic Range; deep structure, seismicity, and GPS motion. *Geology*, *41*(3), 307–310. https://doi.org/10.1130/G33733.1

Martin-Rojas, I. (2022). RINEX files for Insights of active extension within a collisional orogen from GNSS (Central Betic Cordillera, S Spain). [Dataset]. Mendeley Data, V1. https://doi.org/10.17632/bt63fx2ynf.1

Mateos, R. M., Ezquerro, P., Luque-Espinar, J. A., Béjar-Pizarro, M., Notti, D., Azañón, J. M., et al. (2017). Multiband PSInSAR and long-period monitoring of land subsidence in a strategic detrital aquifer (Vega de Granada, SE Spain): An approach to support management decisions. *Journal of Hydrology*, *553*, 71–87. https://doi.org/10.1016/j.jhydrol.2017.07.056

Mazzoli, S., & Helman, M. (1994). Neogene patterns of relative plate motion for Africa-Europe: Some implications for recent central Mediterranean tectonics. *Active continental margins—Present and past* (pp. 464–468). Springer Berlin Heidelberg. https://doi.org/10.1007/978-3-662-38521-0_19

McClusky, S., Reilinger, R., Mahmoud, S., Ben Sari, D., & Tealeb, A. (2003). GPS constraints on Africa (Nubia) and Arabia plate motions. *Geophysical Journal International*, *155*(1), 126–138. https://doi.org/10.1046/j.1365-246X.2003.02023.x

McClymont, A. F., Villamor, P., & Green, A. G. (2009). Fault displacement accumulation and slip rate variability within the Taupo Rift (New Zealand) based on trench and 3-D ground-penetrating radar data. *Tectonics*, *28*(4), TC4005. https://doi.org/10.1029/2008TC002334

Medaouri, M., Déverchère, J., Graindorge, D., Bracene, R., Badji, R., Ouabadi, A., et al. (2014). The transition from Alboran to Algerian basins (Western Mediterranean Sea): Chronostratigraphy, deep crustal structure and tectonic evolution at the rear of a narrow slab rollback system. *Journal of Geodynamics*, *77*, 186–205. https://doi.org/10.1016/j.jog.2014.01.003

Medina-Cascales, I., García-Tortosa, F. J., Martin-Rojas, I., Pérez-Peña, J. V., & Alfaro, P. (2021). Tectonic geomorphology of an active slow-moving, intrabasinal fault: The Galera Fault (Guadix-Baza Basin, central Betic Cordillera, southern Spain). *Geomorphology*, *393*, 107941. https://doi.org/10.1016/j.geomorph.2021.107941

Medina-Cascales, I., Martin-Rojas, I., Peláez Montilla, J. A., García Tortosa, F. J., & Alfaro, P. (2020). Geometry and kinematics of the Baza Fault (central Betic Cordillera, south Spain): Insights into its seismic potential. *Geológica Acta*, *18*(1), 1–25. https://doi.org/10.1344/geologicaacta2020.18.11

Meier, T., Rische, M., Endrun, B., Vafidis, A., & Harjes, H. (2004). Seismicity of the Hellenic subduction zone in the area of Western and central Crete observed by temporary local seismic networks. *Tectonophysics*, *383*(3), 149–169. https://doi.org/10.1016/j.tecto.2004.02.004

Morales, J., Serrano, I., Vidal, F., & Torcal, F. (1997). The depth of the earthquake activity in the Central Betics (Southern Spain). *Geophysical Research Letters*, *24*(24), 3289–3292. https://doi.org/10.1029/97GL03304

Morales, J., Vidal, F., De Miguel, F., Alguacil, G., Posadas, A. M., Ibañez, J. M., et al. (1990). Basement structure of the Granada Basin, Betic Cordilleras, southern Spain. *Tectonophysics*, *177*(4), 337–348. https://doi.org/10.1016/0040-1951(90)90394-N

Morley, C. K., Haranya, C., Phoosongsee, W., Pongwapee, S., Kornsawan, A., & Wonganan, N. (2004). Activation of rift oblique and rift parallel pre-existing fabrics during extension and their effect on deformation style: Examples from the rifts of Thailand. *Journal of Structural Geology*, *26*(10), 1803–1829. https://doi.org/10.1016/j.jsg.2004.02.014

Nicol, A., Walsh, J. J., Villamor, P., Seebeck, H., & Berryman, K. R. (2010). Normal fault interactions, paleoearthquakes and growth in an active rift. *Journal of Structural Geology*, *32*(8), 1101–1113. https://doi.org/10.1016/j.jsg.2010.06.018

Niemi, N. A., Wernicke, B. P., Friedrich, A. M., Simons, M., Bennett, R. A., & Davis, J. L. (2004). BARGEN continuous GPS data across the eastern Basin and Range province, and implications for fault system dynamics. *Geophysical Journal International*, *159*(3), 842–862. https://doi.org/10.1111/j.1365-246X.2004.02454.x

Nocquet, J. (2012). Present-day kinematics of the Mediterranean: A comprehensive overview of GPS results. *Tectonophysics*, *579*, 220–242. https://doi.org/10.1016/j.tecto.2012.03.037

Nocquet, J., & Calais, E. (2003). Crustal velocity field of Western Europe from permanent GPS array solutions, 1996–2001. *Geophysical Journal International*, *154*(1), 72–88. https://doi.org/10.1046/j.1365-246X.2003.01935.x

Notti, D., Mateos, R. M., Monserrat, O., Devanthéry, N., Peinado, T., Roldán, F. J., et al. (2016). Lithological control of land subsidence induced by groundwater withdrawal in new urban AREAS (Granada Basin, SE Spain). Multiband DInSAR monitoring. *Hydrological Processes*, *30*(13), 2317–2331. https://doi.org/10.1002/hyp.10793

Nur, A., & Mavko, G. (1974). Postseismic viscoelastic rebound. *Science*, *183*(4121), 204–206. https://doi.org/10.1126/science.183.4121.204

Oskin, M., Perg, L., Shelef, E., Strane, M., Gurney, E., Singer, B., & Zhang, X. (2008). Elevated shear zone loading rate during an earthquake cluster in eastern California. *Geology*, *36*(6), 507–510. https://doi.org/10.1130/G24814A.1

Palano, M., González, P. J., & Fernández, J. (2015). The Diffuse Plate boundary of Nubia and Iberia in the Western Mediterranean: Crustal deformation evidence for viscous coupling and fragmented lithosphere. *Earth and Planetary Science Letters*, *430*, 439–447. https://doi.org/10.1016/j.epsl.2015.08.040

Pérez-Peña, A., Martín-Davila, J., Gárate, J., Berrocoso, M., & Buforn, E. (2010). Velocity field and tectonic strain in Southern Spain and surrounding areas derived from GPS episodic measurements. *Journal of Geodynamics*, *49*(3), 232–240. https://doi.org/10.1016/j.jog.2010.01.015

Pérez-Peña, J. V., Azañón, J. M., Azor, A., Tuccimei, P., Della Seta, M., & Soligo, M. (2009). Quaternary landscape evolution and erosion rates for an intramontane Neogene basin (Guadix–Baza basin, SE Spain). *Geomorphology*, *106*(3), 206–218. https://doi.org/10.1016/j.geomorph.2008.10.018

Pérouse, E., Vernant, P., Chéry, J., Reilinger, R., & McClusky, S. (2010). Active surface deformation and sub-lithospheric processes in the Western Mediterranean constrained by numerical models. *Geology*, *38*(9), 823–826. https://doi.org/10.1130/G30963.1

Petit, C., Le Pourhiet, L., Scalabrino, B., Corsini, M., Bonnin, M., & Romagny, A. (2015). Crustal structure and gravity anomalies beneath the Rif, northern Morocco: Implications for the current tectonics of the Alboran region. *Geophysical Journal International*, *202*(1), 640–652. https://doi.org/10.1093/gji/ggv169

Phillips, T. B., Jackson, C. A., Bell, R. E., Duffy, O. B., & Fossen, H. (2016). Reactivation of intrabasement structures during rifting: A case study from offshore southern Norway. *Journal of Structural Geology*, *91*, 54–73. https://doi.org/10.1016/j.jsg.2016.08.008

Reicherter, K., Jabaloy, A., Galindo-Zaldívar, J., Ruano, P., Becker-Heidmann, P., Morales, J., et al. (2003). Repeated palaeoseismic activity of the Ventas de Zafarraya fault (S Spain) and its relation with the 1884 Andalusian earthquake. *International Journal of Earth Sciences: Geologische Rundschau*, *92*(6), 912–922. https://doi.org/10.1007/s00531-003-0366-3

Riley, C., & Moore, J. M. (1993). Digital elevation modelling in a study of the neotectonic geomorphology of the Sierra Nevada, southern Spain. *Recent Advances, Zeitschrift für Geomorphologie*, *94*, 25–39.

Ring, U. (1994). The influence of preexisting structure on the evolution of the Cenozoic Malawi rift (East African rift system). *Tectonics*, *13*(2), 313–326. https://doi.org/10.1029/93TC03188

Rodriguez-Fernandez, J., & Sanz de Galdeano, C. (2006). Late orogenic intramontane basin development: The Granada basin, Betics (southern Spain). *Basin Research*, *18*(1), 85–102. https://doi.org/10.1111/j.1365-2117.2006.00284.x

Rohais, S., Eschard, R., Ford, M., Guillocheau, F., & Moretti, I. (2007). Stratigraphic architecture of the Plio-Pleistocene infill of the Corinth rift: Implications for its structural evolution. *Tectonophysics*, *440*(1), 5–28. https://doi.org/10.1016/j.tecto.2006.11.006

Rosenbaum, G., Lister, G. S., & Duboz, C. (2002). Relative motions of Africa, Iberia and Europe during Alpine orogeny. *Tectonophysics*, *359*(1), 117–129. https://doi.org/10.1016/S0040-1951(02)00442-0

Royden, L. H. (1993). Evolution of retreating subduction boundaries formed during continental collision. *Tectonics*, *12*(3), 629–638. https://doi.org/10.1029/92TC02641

Ruano, P., Galindo-Zaldívar, J., & Jabaloy, A. (2004). Recent tectonic structures in a transect of the Central Betic Cordillera. *Pure and Applied Geophysics*, *161*(3), 541–563. https://doi.org/10.1007/s00024-003-2462-5

Ruiz, A. M., Ferhat, G., Alfaro, P., Sanz de Galdeano, C., Lacy, M. C., Rodríguez-Caderot, G., & Gil, A. J. (2003). Geodetic measurements of crustal deformation on NW–SE faults of the Betic Cordillera, southern Spain, 1999–2001. *Journal of Geodynamics*, *35*(3), 259–272. https://doi.org/10.1016/S0264-3707(02)00134-5

Salomon, E., Koehn, D., & Passchier, C. (2015). Brittle reactivation of ductile shear zones in NW Namibia in relation to South Atlantic rifting. *Tectonics*, *34*(1), 70–85. https://doi.org/10.1002/2014TC003728

Santamaría-Gómez, A. (2019). SARI: Interactive GNSS position time series analysis software. *GPS Solutions*, *23*(2), 1–6. https://doi.org/10.1007/s10291-019-0846-y

Sanz de Galdeano, C., & Alfaro, P. (2004). Tectonic significance of the present relief of the Betic Cordillera. *Geomorphology*, *63*(3), 175–190. https://doi.org/10.1016/j.geomorph.2004.04.002

Sanz de Galdeano, C., Azañón, J. M., Cabral, J., Ruano, P., Alfaro, P., Canora, C., et al. (2020). Active Faults in Iberia. In C. Quesada, & J. T. Oliveira (Eds.), *The geology of Iberia: A geodynamic approach: Volume 5: Active processes: Seismicity, active faulting and relief* (pp. 33–75). Springer International Publishing. https://doi.org/10.1007/978-3-030-10931-8_4

Sanz de Galdeano, C., García-Tortosa, F. J., Peláez, J. A., Alfaro, P., Azañón, J. M., Galindo-Zaldívar, J., et al. (2012). Main active faults in the Granada and Guadix-Baza Basins (Betic Cordillera)/Principales fallas activas de las Cuencas de Granada y Guadix-Baza (Cordillera Bética). *Journal of Iberian Geology*, *38*(1), 209. Retrieved from https://search.proquest.com/docview/1095127976

Sanz de Galdeano, C., & López-Garrido, A. C. (1999). Nature and impact of the Neotectonic deformation in the western Sierra Nevada (Spain). *Geomorphology*, *30*(3), 259–272. https://doi.org/10.1016/S0169-555X(99)00034-3

Sanz de Galdeano, C., Montilla, P. J. A., & López Casado, C. (2003). Seismic potential of the main active faults in the Granada Basin (Southern Spain). *Pure and Applied Geophysics*, *160*(8), 1537–1556. https://doi.org/10.1007/s00024-003-2359-3

Savage, J. C., & Prescott, W. H. (1978). Asthenosphere readjustment and the earthquake cycle. *Journal of Geophysical Research*, *83*(B7), 3369–3376. https://doi.org/10.1029/JB083iB07p03369

Schlagenhauf, A., Gaudemer, Y., Benedetti, L., Manighetti, I., Palumbo, L., Schimmelpfennig, I., et al. (2010). Using in situ Chlorine-36 cosmonuclide to recover past earthquake histories on limestone normal fault scarps: A reappraisal of methodology and interpretations. *Geophysical Journal International*, *182*(1), 36–72. https://doi.org/10.1111/j.1365-246X.2010.04622.x

Serpelloni, E., Vannucci, G., Pondrelli, S., Argnani, A., Casula, G., Anzidei, M., et al. (2007). Kinematics of the Western Africa-Eurasia plate boundary from focal mechanisms and GPS data. *Geophysical Journal International*, *169*(3), 1180–1200. https://doi.org/10.1111/j.1365-246X.2007.03367.x

Silva, P. G., Goy, J. L., Zazo, C., & Bardají, T. (2003). Fault-Generated mountain fronts in southeast Spain: Geomorphologic assessment of tectonic and seismic activity. *Geomorphology*, *50*(1), 203–225. https://doi.org/10.1016/S0169-555X(02)00215-5

Smith, R. B., & Sbar, M. L. (1974). Contemporary tectonics and seismicity of the Western United States with Emphasis on the Intermountain seismic Belt. *Geological Society of America Bulletin*, *85*(8), 1205–1218. https://doi.org/10.1130/0016-7606(1974)85\2.0.CO;2

Soto, J. I., Fernández-Ibáñez, F., Fernàndez, M., & García-Casco, A. (2008). Thermal structure of the crust in the Gibraltar Arc: Influence on active tectonics in the western Mediterranean. *Geochemistry, Geophysics, Geosystems*, *9*(10), Q10011. https://doi.org/10.1029/2008GC002061

Sousa, J. J., Ruiz, A. M., Hanssen, R. F., Bastos, L., Gil, A. J., Galindo-Zaldívar, J., & Sanz de Galdeano, C. (2010). PS-InSAR processing methodologies in the detection of field surface deformation—Study of the Granada Basin (Central Betic Cordilleras, southern Spain). *Journal of Geodynamics*, *49*(3), 181–189. https://doi.org/10.1016/j.jog.2009.12.002

Spakman, W., Chertova, M. V., van den Berg, A., & van Hinsbergen, D. J. J. (2018). Puzzling features of western Mediterranean tectonics explained by slab dragging. *Nature Geoscience*, *11*, 211–216. https://doi.org/10.1038/s41561-018-0066-z

Srivastava, S. P., Roest, W. R., Kovacs, L. C., Oakey, G., Lévesque, S., Verhoef, J., & Macnab, R. (1990). Motion of Iberia since the Late Jurassic: Results from detailed aeromagnetic measurements in the Newfoundland Basin. *Tectonophysics*, *184*(3), 229–260. https://doi.org/10.1016/0040-1951(90)90442-B

Stich, D., Martín, J. B., & Morales, J. (2007). Deformación sísmica y asísmica en la zona Béticas-Rif-Alborán. *Revista de la Sociedad Geológica de España*, *20*(3–4), 311–319.

Stich, D., Serpelloni, E., de Lis Mancilla, F., & Morales, J. (2006). Kinematics of the Iberia–Maghreb plate contact from seismic moment tensors and GPS observations. *Tectonophysics*, *426*(3), 295–317. https://doi.org/10.1016/j.tecto.2006.08.004

Taylor, B., Weiss, J. R., Goodliffe, A. M., Sachpazi, M., Laigle, M., & Hirn, A. (2011). The structures, stratigraphy and evolution of the Gulf of Corinth rift, Greece. *Geophysical Journal International*, *185*(3), 1189–1219. https://doi.org/10.1111/j.1365-246X.2011.05014.x

Tendero-Salmerón, V. (2022). Recent and active deformation structures in the central-eastern sector of the Betic Cordillera and the Alboran Sea: Indentation processes and roll-back.

Tong, X., Smith-Konter, B., & Sandwell, D. T. (2014). Is there a discrepancy between geological and geodetic slip rates along the San Andreas Fault System? *Journal of Geophysical Research: Solid Earth*, *119*(3), 2518–2538. https://doi.org/10.1002/2013JB010765

Velasco, M. S., Bennett, R. A., Johnson, R. A., & Hreinsdóttir, S. (2010). Subsurface fault geometries and crustal extension in the eastern Basin and Range Province, Western U.S. *Tectonophysics*, *488*(1), 131–142. https://doi.org/10.1016/j.tecto.2009.05.010

Ziegler, P. A. (1992). North Sea rift system. *Tectonophysics*, *208*(1), 55–75. https://doi.org/10.1016/0040-1951(92)90336-5